



**González-Gil, Ricardo and González Taboada, Fernando and Cáceres, Carlos and Largier, John L. and Anadón, Ricardo (2017) Winter-mixing preconditioning of the spring phytoplankton bloom in the Bay of Biscay. *Limnology and Oceanography*. ISSN 0024-3590 , <http://dx.doi.org/10.1002/lno.10769>**

This version is available at <https://strathprints.strath.ac.uk/63473/>

**Strathprints** is designed to allow users to access the research output of the University of Strathclyde. Unless otherwise explicitly stated on the manuscript, Copyright © and Moral Rights for the papers on this site are retained by the individual authors and/or other copyright owners. Please check the manuscript for details of any other licences that may have been applied. You may not engage in further distribution of the material for any profitmaking activities or any commercial gain. You may freely distribute both the url (<https://strathprints.strath.ac.uk/>) and the content of this paper for research or private study, educational, or not-for-profit purposes without prior permission or charge.

Any correspondence concerning this service should be sent to the Strathprints administrator: [strathprints@strath.ac.uk](mailto:strathprints@strath.ac.uk)

1 **Winter-mixing preconditioning of the spring phytoplankton bloom in**  
2 **the Bay of Biscay**

3 **Authors:** Ricardo González-Gil<sup>1\*</sup>, Fernando González Taboada<sup>2,3</sup>, Carlos Cáceres<sup>4</sup>, John L.  
4 Largier<sup>5</sup>, Ricardo Anadón<sup>1</sup>

5 \* Contact author e-mail: [rgonzalezgil@gmail.com](mailto:rgonzalezgil@gmail.com)

6 1. Área de Ecología, Dpto. Biología de Organismos y Sistemas, Universidad de Oviedo, C/Valentín Andrés Álvarez  
7 s/n, E33071 Oviedo, Asturias, Spain.

8 2. Atmospheric and Oceanic Sciences, Princeton University, Princeton, NJ, USA.

9 3. Geophysical Fluid Dynamics Laboratory, National Oceanic and Atmospheric Administration, Princeton, NJ  
10 08540 USA.

11 4. Dept. of Mathematics and Statistics, University of Strathclyde, 26 Richmond St, Glasgow G1 1XQ, UK

12 5. Bodega Marine Laboratory, University of California, Davis, 2099 Westside Drive, Bodega Bay, CA 94923-0247  
13 USA.

14 **Running head:** Winter mixing and spring bloom

15 **Key words:** winter mixing, spring phytoplankton bloom, time series, global warming, remote  
16 sensing, Bay of Biscay  
17

18      **Abstract**

19      The spring phytoplankton bloom plays a key role in the dynamics of temperate and  
20 polar seas. Nevertheless, the mechanisms and processes behind these blooms remain a  
21 subject of considerable debate. We analyzed the influence of deep mixing during winter  
22 on the spring phytoplankton bloom in the Cantabrian Sea (southern Bay of Biscay). To  
23 this end, we combined long-term physical and biogeochemical in situ data (1993-2012)  
24 and satellite observations (1997-2012). Deeper winter mixing led to higher nitrate and  
25 chlorophyll concentrations through the water column during the spring bloom. However,  
26 this effect was modified by short-term variability in near-surface stratification in spring.  
27 Winter-mixing preconditioning also influenced different spring bloom metrics: deeper  
28 and later mixing in winter was followed by later blooms with a larger peak. In these  
29 enhanced blooms, nitrate was taken up at faster rates, indicating higher rates of  
30 phytoplankton production. Winters with weaker mixing (that led to weaker spring  
31 blooms) were associated with warmer surface temperatures. This relationship suggests  
32 that the multi-decadal trend towards warmer surface temperatures in the Bay of Biscay  
33 may promote a decrease in the magnitude of the spring bloom, which could impact upper  
34 trophic levels and also deep carbon export in the future.

## 35 **Introduction**

36 Every year, the spring phytoplankton bloom reappears in temperate and polar seas,  
37 turning surface waters green. This phenomenon has fascinated researchers since the early  
38 days of oceanography in the 19<sup>th</sup> century (Banse 1992; Fischer et al. 2014). In the last  
39 decades, satellite images of surface chlorophyll concentration led to a renewed interest in  
40 phytoplankton blooms by revealing their ubiquity and large spatial extent (Parsons and  
41 Lalli 1988; Yoder et al. 1993; McClain 2009). Vernal phytoplankton blooms pump  
42 important amounts of atmospheric carbon into deep oceanic waters, making them a key  
43 component of biogeochemical cycles (Longhurst and Harrison 1989; Falkowski et al.  
44 1998; Sarmiento and Gruber 2006). At the same time, these blooms support much of the  
45 annual productivity at higher trophic levels, including many exploited species (Hjort  
46 1914; Cushing 1990; Townsend et al. 1994).

47 The North Atlantic spring phytoplankton bloom is the most pronounced bloom in open  
48 ocean waters (Yoder et al. 1993), although its characteristics vary substantially in space  
49 and time (Ueyama and Monger 2005; Racault et al. 2012; González Taboada and Anadón  
50 2014). Interannual changes in the timing and magnitude of phytoplankton blooms can  
51 lead to a trophic match-mismatch that modulates the survival of upper trophic levels,  
52 including commercially fished stocks (Cushing 1990; Platt et al. 2003; Durant et al. 2007;  
53 Koeller et al. 2009; Kristiansen et al. 2011). With such important impacts, there is a  
54 growing interest in understanding the factors that promote interannual variability in the  
55 characteristics of the spring phytoplankton bloom, especially in the context of global  
56 climate change (Racault et al. 2012). Different hypotheses have been proposed to explain  
57 the mechanisms that trigger the onset of spring blooms, leading to an intense and ongoing  
58 debate (Behrenfeld and Boss 2014; Lindemann and St. John 2014; Chiswell et al. 2015;

This is the accepted version of the following article: González-Gil, R., González Taboada, F., Cáceres, C., Largier, J. L. and Anadón, R. (2017), Winter-mixing preconditioning of the spring phytoplankton bloom in the Bay of Biscay. *Limnol. Oceanogr.* doi:10.1002/lno.10769, which has been published in final form at [Limnology & Oceanography](#). This article may be used for non-commercial purposes in accordance with the [Wiley Self-Archiving Policy](#).

59 Ferreira et al. 2015). Most of the drivers involved in these mechanisms also influence the  
60 magnitude of the bloom (Follows and Dutkiewicz 2002; Henson et al. 2006; Henson et  
61 al. 2009).

62 Among the physical processes that influence bloom development, deep mixing in  
63 winter stands out due to its crucial role in preconditioning the environment for a  
64 phytoplankton bloom in the next spring. During winter, deep convective mixing leads to  
65 the replenishment of near-surface nutrients (Williams and Follows 2003). Inorganic  
66 nitrogen compounds, such as nitrate, are often limiting for phytoplankton productivity  
67 (Falkowski et al. 1998; Moore et al. 2013) and thus, their availability is an important  
68 factor controlling the development of spring blooms (see for example Sambrotto et al.  
69 1986; Sieracki et al. 1993; D'Ortenzio et al. 2014). As winter progresses towards spring,  
70 nutrients in surface layers become isolated from deeper waters with the onset of seasonal  
71 stratification. This sets an upper bound on the amount of nutrients available for  
72 phytoplankton in spring because, for many species, the access to nutrients below the  
73 seasonal thermocline is very limited. Deep mixing also constrains phytoplankton growth  
74 and the density of seeding populations by reducing the residence time of individual  
75 phytoplankters in the euphotic layer (Sverdrup 1953), although it simultaneously  
76 decreases encounter rates with grazers due to dilution effects (Yoshie et al. 2003;  
77 Behrenfeld 2010; Behrenfeld and Boss 2014).

78 With such a variety of effects operating together, the question that arises is: how and  
79 to what extent does winter mixing influence the spring phytoplankton bloom? Several  
80 studies have investigated the role of winter mixing in determining the magnitude of spring  
81 blooms (e.g. Follows and Dutkiewicz 2002; Henson et al. 2009; Martinez et al. 2011), but  
82 we are not aware of any analyses of how winter mixing affects other characteristics such

83 as bloom timing and duration. In addition, phytoplankton blooms are usually analyzed  
84 either in terms of changes in surface or in depth-integrated chlorophyll, ignoring potential  
85 changes in vertical structure (Chiswell et al. 2015). Indeed, phytoplankton community  
86 structure varies consistently across vertical gradients in the water column, with marked  
87 changes in physiological, ecological and taxonomic patterns (Reynolds 2006).

88 A proper characterization of spring phytoplankton blooms demands high frequency  
89 sampling to capture rapid changes in phytoplankton biomass (Rantajarvi et al. 1998). This  
90 imposes a major constraint on analyses of change in phytoplankton phenology. The  
91 availability of daily satellite ocean color measurements only partially alleviates this  
92 problem, given the lack of data during cloudy periods and the limitation of measurements  
93 to surface waters (McClain 2009). On the other hand, traditional approaches based on in  
94 situ sampling allow the collection of information at different depths, but sustained  
95 sampling based on recurrent oceanographic cruises spanning many years is limited to  
96 lower frequency sampling (Karl 2010; Church et al. 2013).

97 We combined monthly in situ data (1993-2012) with quasi-daily satellite observations  
98 (1997-2012) to analyze the influence of deep winter mixing on the spring phytoplankton  
99 bloom in the central Cantabrian Sea (southern Bay of Biscay). In this temperate sea,  
100 nutrient supply to upper layers is largely driven by deep mixing processes during winter  
101 (Llope et al. 2007; Hartman et al. 2013), leading to a well-developed spring bloom that is  
102 a major feature of the seasonal cycle of phytoplankton (Varela 1996). First, we examined  
103 the relationship of winter mixing with nitrate and phytoplankton concentrations through  
104 the water column during the spring bloom, considering also short-term variability in the  
105 stability of the upper layer. Next, we assessed how inter-annual changes in winter mixing  
106 modulate the timing, duration and intensity of the surface expression of the spring bloom.

This is the accepted version of the following article: González-Gil, R., González Taboada, F., Cáceres, C., Largier, J. L. and Anadón, R. (2017), Winter-mixing preconditioning of the spring phytoplankton bloom in the Bay of Biscay. *Limnol. Oceanogr.* doi:10.1002/lno.10769, which has been published in final form at [Limnology & Oceanography](#). This article may be used for non-commercial purposes in accordance with the [Wiley Self-Archiving Policy](#).

107 Finally, we explored how changes in surface temperature impacts the development of the  
108 spring phytoplankton bloom through its influence on winter mixing. Through these  
109 analyses, we assess the relative importance of winter mixing on the interannual variability  
110 of the spring phytoplankton bloom in temperate seas.

111

## 112 **Material and methods**

113 The central Cantabrian Sea (southern Bay of Biscay, Fig. 1) has been sampled  
114 intensively for the last two decades as part of the Spanish long-term monitoring network  
115 RADIALES ([www.seriestemporales-ieo.com](http://www.seriestemporales-ieo.com), Valdés et al. 2002; Valdés et al. 2007).  
116 Here, we used samples collected monthly between 1993 and 2012 at station E3, the most  
117 oceanic station of the Cudillero transect. Station E3 is located close to the shelf break,  
118 over the Avilés Canyon (06°10'W, 43°46'N, depth 870 m), and it reflects oceanic  
119 conditions typical of a temperate sea. A detailed description of the station and information  
120 about the protocols used can be found in Llope et al. (2006). We combined these in situ  
121 samples with daily satellite data for surface chlorophyll a concentration ([Chl a]<sub>SAT</sub>) and  
122 sea surface temperature (SST) averaged over a 0.25° quadrangular pixel centered at  
123 6.125°W and 43.875°N (Fig. 1).

### 124 **In situ oceanographic observations**

125 We used 500-m CTD profiles (SeaBird-25) to assess the intensity of winter mixing  
126 between 1993 and 2012. We estimated mixed layer depth (hereafter MLD<sub>0.5</sub>) as the depth  
127 where the temperature decreases 0.5°C with respect to the temperature at 10 m depth  
128 (Monterey and Levitus 1997). Then, we determined annual maximum winter mixing  
129 depths (WMD<sub>max</sub>) from MLD<sub>0.5</sub> estimates in winter months (January, February or March),  
130 before the spring [Chl a]<sub>SAT</sub> maximum (see Statistical analysis and spring bloom metrics  
131 section). Incomplete profiles or those showing a thermal inversion were rejected to avoid  
132 under- or over-estimating MLD<sub>0.5</sub>, respectively. Thermal inversions were identified in  
133 profiles where temperatures exceeded the 10-m-depth temperature by 0.1°C or more over  
134 at least 25 m. It is important to note that, due to the monthly sampling frequency, the deep



135 mixing process leading to the measured  $WMD_{max}$  could have occurred days or weeks  
136 before the monthly sampling date, or that later events could lead to deeper mixing before  
137 sampling the next profile.

138 Short-term changes in near-surface stratification can mask the influence of winter  
139 mixing on spring bloom characteristics. To control for this masking effect, we included  
140 the estimated depth of near-surface stratification in our analysis. We estimated the depth  
141 of the near-surface stratification (hereafter  $MLD_{0.1}$ ) on each sampling date from the depth  
142 at which temperature is  $0.1^{\circ}C$  lower than at 4 m depth (or at 6 m depth, if 4 m was missing;  
143 see Dever et al. 2006; Chiswell 2011; Houpert et al. 2015). Daily variations in the near-  
144 surface stratification depth affect phytoplankton vertical distribution and the local  
145 conditions experienced by phytoplankton cells during the spring bloom (Chiswell 2011;  
146 Chiswell et al. 2015; Franks 2015). Heating of surface water is the primary source of  
147 stratification, which suppresses near-surface turbulence (Franks 2015). Therefore, the  
148 depth of thermal stratification largely controls how far phytoplankton cells can be moved  
149 away from the surface and thus determines the amount of light received by phytoplankton.

150 We examined changes in observed nitrate and chlorophyll a (Chl a) concentrations in  
151 the upper 200 m to analyze the potential bottom-up effects of winter mixing on spring  
152 phytoplankton blooms. Nitrate is the most limiting nutrient of phytoplankton growth in  
153 the area (Llope et al. 2007), while Chl a data were used as a proxy for phytoplankton  
154 biomass. Both nitrate and Chl a samples were collected at eight depths (~ 0, 10, 20, 30,  
155 40, 50, 75, 100, 150, 200 m) at station E3 using 5-L Niskin bottles. Nitrate samples were  
156 frozen and stored at  $-20^{\circ}C$  before measuring nitrate concentrations using a Technicon  
157 AAI Autoanalyser (Industrial Method 158-71 W/A) and a Skalar SANplus (Skalar  
158 Analytical B.V.). Post-cruise nitrate concentrations were converted from  $\mu mol L^{-1}$  to

159  $\mu\text{mol kg}^{-1}$  using water density estimates at average laboratory conditions (22.5°C and  
160 98.6 kPa at 232 m.a.s.l.). Chl a concentrations were estimated by filtering samples  
161 through GF-F filters (25 mm diameter), using 200 mL for low-Chl a samples, and 100  
162 mL for high-Chl a samples. These filters were subsequently frozen at -20°C. Then, Chl a  
163 was extracted in 10 mL of 90% acetone over 24 h in darkness at 4°C. Chl a concentrations  
164 were measured using a Turner Designs 10 fluorometer following the method of Yentsch  
165 and Menzel (1963).

166 We explored seasonal and interannual variability in Chl a and nitrate concentrations  
167 through the water column using contour plots based on kriging interpolation (Nychka et  
168 al. 2015). Before kriging, we used linear interpolation to ensure that the shape of vertical  
169 profiles was locally preserved in the contour plots (i.e. by estimating concentrations every  
170 two meters). We also used linear interpolation to estimate missing Chl a and nitrate  
171 concentrations in the profile of a given date before calculating depth-integrated values.  
172 Linear interpolation was preceded by a  $\log_{10}$  transformation of Chl a concentrations. To  
173 avoid unreliable estimates, we discarded profiles containing only one data point. We  
174 calculated depth-integrated Chl a and nitrate using the trapezoidal rule. Depth-integrated  
175 Chl a was calculated for ~0 to 200 m depth and regarded as a proxy of total phytoplankton  
176 biomass in the water column. Nitrate was integrated from ~ 0 to 50 m depth, just below  
177 the nitracline depth during the seasonal stratification (see Figs. 2 and 3). Nitrate in this  
178 upper layer is extensively exploited by phytoplankton during the spring bloom. The  
179 nitracline was defined by a threshold concentration of  $1 \mu\text{mol kg}^{-1}$ , following Cullen and  
180 Eppley (1981).

181

## Remote sensing data

182 We used a time series of remotely sensed surface Chl a concentration ([Chl a]<sub>SAT</sub>) to  
183 characterize the development of the spring phytoplankton bloom. In temperate latitudes,  
184 [Chl a]<sub>SAT</sub> provides a reliable proxy of phytoplankton biomass (McClain 2009). Satellite  
185 retrievals were averaged over a 0.25 x 0.25° quadrangle covering station E3 (Fig. 1). Daily  
186 time series of [Chl a]<sub>SAT</sub> between September 1997 and December 2012 were retrieved  
187 from Level 3 (geolocated, corrected and averaged over a regular grid) SeaWiFS (Sept.  
188 1997-Dec. 2007, reprocessing R2010.0) and Aqua MODIS (Jul. 2002-Dec. 2012,  
189 reprocessing R2013.1.1) standard mapped images (SMI) available at the Ocean Color  
190 Web (NASA OBPG 2015a; b). Estimates of [Chl a]<sub>SAT</sub> were derived using version six of  
191 the OC4 (SeaWiFS) and OC3M (Aqua MODIS) empirical band-ratio algorithms  
192 (O'Reilly et al. 2000, [oceancolor.gsfc.nasa.gov/cms/atbd/chlor\\_a](http://oceancolor.gsfc.nasa.gov/cms/atbd/chlor_a)).

193 We also used remotely sensed sea surface temperature (SST, see Statistical analysis  
194 and spring bloom metrics section). The SST time series (from September 1981 to  
195 December 2012) was derived from the NOAA-Optimum Interpolation 1/4 Degree Daily  
196 Sea Surface Temperature Analysis (OISST version 2). The methods are described in  
197 Reynolds et al. (2007). The database of SST images is produced and maintained by C.  
198 Liu and R. W. Reynolds at NCDC ([www.ncdc.noaa.gov/oisst](http://www.ncdc.noaa.gov/oisst)). SST is one of the most  
199 important parameters in the dynamics of pelagic ecosystems: it has a direct effect on  
200 metabolic rates (Eppley 1972; Ikeda 1985), and it is an indicator of many physical  
201 processes that affect pelagic organisms, such as mixing and upwelling. Thus, we also  
202 explored the relationship between SST and the intensity of mixing in winter.

203

## Statistical analysis and spring bloom metrics

204 The characterization of the spring phytoplankton bloom and the influence of winter  
205 mixing differed depending on whether in situ data or remotely sensed data were used. In  
206 the case of in situ sampling, the availability of data through the entire water column  
207 allowed us to study variations in the development of the bloom at different depths,  
208 considering also concomitant changes in nitrate concentration. On the other hand, higher  
209 frequency satellite data allowed extraction of different bloom metrics, although this  
210 approach was restricted to surface waters. To conduct our analyses, we combined simple  
211 linear regressions and Generalized Additive Models (GAMs, Hastie and Tibshirani 1990).  
212 The main characteristic of GAMs is the inclusion of unspecified smooth functions to  
213 capture nonlinear relationships among the response and predictor variables (see  
214 Supporting information for further details). We assumed independent and identically  
215 distributed normal errors in all cases, which required  $\log_{10}$  transformation of Chl a data  
216 before the analyses (both in situ and satellite). Model assumptions were checked by  
217 examining the distribution of residuals. All the statistical analyses were performed in R  
218 version 3.3.3 (R Core Team 2017) using RStudio interface version 1.0.143 (RStudio  
219 Team 2016). GAMs were fitted using the functions `gam` and `t2` from the package `mgcv`  
220 (v1.8-17, Wood 2006; Wood et al. 2013). We also used the package `LatticeKrig` v6.2  
221 (Nychka et al. 2016) for kriging interpolation. Figures were created using package  
222 `ggplot2` (v2.2.1, Wickham 2009) and graphically improved in Inkscape  
223 ([www.inkscape.org](http://www.inkscape.org)).

224 Characterization of seasonality

225 We characterized the shape of the seasonal cycle for physical variables (SST, MLD<sub>0.5</sub>  
226 and MLD<sub>0.1</sub>), nitrate and Chl a. We fitted the following GAM to each physical variable,  
227 depth-integrated nitrate and Chl a, surface nitrate concentration and [Chl a]<sub>SAT</sub> (all of  
228 them represented below as  $y$ ):

$$y = a + f(t) + \varepsilon \quad (1)$$

229 The model includes an intercept ( $a$ ), a 1D smooth function ( $f$ ) to represent the seasonal  
230 curve as a function of day of the year ( $t$ ) and an error term represented by  $\varepsilon$  (see  
231 Supporting information for further specifications).

232 In the case of in situ Chl a and nitrate concentration, we estimated the seasonality  
233 through the water column using a GAM that included an interaction term between the day  
234 of the year ( $t$ ) and depth ( $z$ ):

$$y = a + te(t, z) + \varepsilon \quad (2)$$

235 where the interaction term  $te(t, z)$  is a 2D smooth function (specifically, a tensor  
236 product) that captures the seasonal cycle of the vertical profiles of Chl a and nitrate  
237 concentration over the day of the year (Wood 2006).

238 Analysis of the winter mixing effect based on in situ data

239 We first inspected the effect of deep mixing on depth-integrated nitrate in winter using  
240 a simple linear regression. Then, to examine the influence of winter mixing on spring-

This is the accepted version of the following article: González-Gil, R., González Taboada, F., Cáceres, C., Largier, J. L. and Anadón, R. (2017), Winter-mixing preconditioning of the spring phytoplankton bloom in the Bay of Biscay. *Limnol. Oceanogr.* doi:10.1002/lno.10769, which has been published in final form at [Limnology & Oceanography](#). This article may be used for non-commercial purposes in accordance with the [Wiley Self-Archiving Policy](#).

241 bloom Chl a and nitrate concentrations through the water column, we identified the month  
 242 with maximum surface Chl a concentration during the first half of each year. We  
 243 considered this month as representative of conditions during the spring bloom. We  
 244 formulated then a set of alternative models to explore the influence of  $WMD_{max}$  and  
 245  $MLD_{0.1}$  on vertical profiles of Chl a and nitrate that month (see Table 1). Alternative  
 246 models were later compared based on Akaike Information Criterion (AIC, Burnham and  
 247 Anderson 2002). The basic null model, which only included an intercept, was expanded  
 248 by adding terms for the influence of depth and for the interaction effect between depth  
 249 and either  $WMD_{max}$  or  $MLD_{0.1}$  (note that  $WMD_{max}$  and  $MLD_{0.1}$  were uncorrelated,  $r =$   
 250  $0.11$ ,  $p$ -value =  $0.688$ ). These interaction terms were included to capture a distinct depth-  
 251 dependent effect of  $WMD_{max}$  or  $MLD_{0.1}$ . We completed the analysis by testing the  
 252 existence of an interaction effect between  $WMD_{max}$  and  $MLD_{0.1}$ , although we limited this  
 253 analysis to surface waters (See Table 2 for the list of models tested). This enabled an  
 254 easier comparison with satellite information. Additionally, we explored this interaction  
 255 effect for depth-integrated Chl a.

256 We concluded the analysis of profile data by examining the impact of winter mixing  
 257 on new primary production ( $PP_{new}$ ) during the spring bloom. Assuming that the effect of  
 258 transport and external sources is negligible, we can ascribe the drawdown of nitrate in the  
 259 upper layers mainly to phytoplankton uptake. This provides a rough approximation of  
 260  $PP_{new}$  ( $mg\ C\ m^{-2}\ day^{-1}$ ) during the bloom:

$$PP_{new} \sim r_{C:N} \int_{50}^0 \frac{1}{\Delta t} ([NO_3]_{z,t_i} - [NO_3]_{z,t_f}) dz \quad (3)$$

261 where the decay in nitrate concentration  $[\text{NO}_3]$  at depth  $z$  ( $\text{mol m}^{-3}$ ) between February  
262 ( $t_i$ ) and April ( $t_f$ ) was integrated over the upper 50 m of the water column (i.e. from just  
263 below the nitracline depth during the seasonal stratification, see Figs. 2 and 3). For each  
264 season, we subtracted nitrate concentrations in February from those recorded in April to  
265 cover the entire bloom development. Differences in  $[\text{NO}_3]$  were averaged over time using  
266 the difference in days between sampling dates,  $\Delta t$ . The factor used in the conversion from  
267 nitrate to carbon units ( $r_{C:N} = 6.6$ ) was based on a constant C:N ratio averaged from the  
268 C:N ratios for the new production estimated by Körtzinger et al. (2001) in bloom and  
269 early bloom sampling stations during a meridional transect carried out in the Northeast  
270 Atlantic. This  $r_{C:N}$  coincides with the ratio described by Redfield (1958) for the  
271 particulate organic matter in the ocean. We calculated  $PP_{new}$  for each season and  
272 compared it with the intensity of winter mixing using a simple linear regression on  
273  $WMD_{max}$  measured during the preceding winter. We presumed that a positive relationship  
274 between  $PP_{new}$  and  $WMD_{max}$  would be indicative of the preconditioning effect of winter  
275 mixing on the spring bloom development.

#### 276 Spring bloom characterization based on satellite data

277 The high temporal resolution of  $[\text{Chl a}]_{SAT}$  data allowed us to extend the analysis of  
278 interannual variability in the spring bloom. To do that, we fitted a GAM featuring a  
279 changing seasonal cycle among years both to  $[\text{Chl a}]_{SAT}$  and SST data ( $y$ ):

$$y = a + f(t|year) + \varepsilon \quad (4)$$

280 where  $a$  corresponds to the intercept,  $t$  to the day of the year, and  $\varepsilon$  is an error term.

281 The  $f(t|year)$  term is included to capture changes in the seasonality among years. In the

This is the accepted version of the following article: González-Gil, R., González Taboada, F., Cáceres, C., Largier, J. L. and Anadón, R. (2017), Winter-mixing preconditioning of the spring phytoplankton bloom in the Bay of Biscay. *Limnol. Oceanogr.* doi:10.1002/lno.10769, which has been published in final form at [Limnology & Oceanography](#). This article may be used for non-commercial purposes in accordance with the [Wiley Self-Archiving Policy](#).

282 model, the seasonal cycle starts in July 15<sup>th</sup> (or 14<sup>th</sup> in a leap year). This choice ensured  
283 that the seasonal term included the annual SST maximum and the SST minimum in the  
284 next year, both required to derive spring bloom metrics (see below). For [Chl a]<sub>SAT</sub>,  
285 analyses conducted beforehand indicated that there is no need to account for differences  
286 in mean concentration or in the shape of the seasonal cycle between sensors (SeaWiFS  
287 and Aqua MODIS). Lack of [Chl a]<sub>SAT</sub> information during the period 1997-1998 resulted  
288 in unreliable estimates of bloom metrics that were not included in the main analyses.

289 We retrieved a series of metrics to characterize interannual changes in the spring  
290 bloom based on modelled time series of [Chl a]<sub>SAT</sub> (Eq. 4). We determined first the timing  
291 of the autumn bloom, which follows the annual SST maximum. The autumn bloom was  
292 defined as the first local maximum in [Chl a]<sub>SAT</sub> reached after at least 30 consecutive days  
293 of increase in [Chl a]<sub>SAT</sub> (this condition prevents confounding this bloom with a small  
294 rise in [Chl a]<sub>SAT</sub>). Then, we defined spring bloom rise as the day when the seasonal curve  
295 of [Chl a]<sub>SAT</sub> increased at the fastest rate following the autumn bloom. If no autumn bloom  
296 was observed (i.e. only one [Chl a]<sub>SAT</sub> maximum occurred), then spring bloom rise was  
297 defined as the date when the [Chl a]<sub>SAT</sub> seasonal curve increased at the fastest rate. This  
298 criterion to identify the timing of the spring bloom avoids the use of an a priori  
299 chlorophyll threshold (for references discussing different criteria, see Brody et al. 2013;  
300 Blondeau-Patissier et al. 2014; González Taboada and Anadón 2014). We defined bloom  
301 decay as the day when the [Chl a]<sub>SAT</sub> seasonal curve decreased at the fastest rate after  
302 both the spring bloom maximum (i.e. the magnitude of the spring bloom peak, max Chl  
303 a) and minimum SST. The latter condition allows identification of the real spring bloom  
304 decay, avoiding confusion with an early, temporary decrease in [Chl a]<sub>SAT</sub> after reaching  
305 the max Chl a. The day of occurrence of the max Chl a was another timing metric (max



306 Chl a day). Finally, we identified the bloom span as the number of days between bloom  
307 rise and bloom decay.

308 Once we calculated these bloom metrics for each year, we inspected the influence of  
309 winter mixing on them by using linear regression analysis. We also used linear  
310 regressions to analyze SST long-term trends and to explore the impact of SST on the  
311 magnitude of winter mixing at different lags.

312

## 313 **Results**

### 314 **Seasonality**

315 Physical variables (SST, MLD<sub>0.5</sub>, MLD<sub>0.1</sub>) and both nitrate and Chl a concentrations  
316 at different depths, or integrated through the water column, all showed a clear seasonal  
317 pattern (Figs. 2 and 3). The seasonal cycle in SST exhibited a maximum of 20.34°C in  
318 August and a minimum of 12.54°C in March (Fig. 3a). In mid-winter (January and  
319 February), both MLD<sub>0.5</sub> and MLD<sub>0.1</sub> were deep, indicating a well-mixed water column  
320 (Fig. 3b). Some profiles showed shallower MLD<sub>0.1</sub> than MLD<sub>0.5</sub> during the well-mixed  
321 period, indicating that transient shallow and weak stratification may develop in winter,  
322 accounting for a shallow MLD<sub>0.1</sub> being observed above a deeper MLD<sub>0.5</sub> that may have  
323 formed days or even weeks before the sampling dates. As a consequence of the mixing,  
324 nitrate was homogeneously distributed through the water column in mid-winter (average  
325 concentration of 4.68  $\mu\text{mol kg}^{-1}$ , Fig. 3c), which accounts for the annual maximum in the  
326 uppermost 50 m (Figs. 3c, 3e and 3g). At the end of February, a surface stratified layer  
327 started to form (shoaling of MLD<sub>0.1</sub>), which is the beginning of seasonal stratification  
328 (Fig. 3b). Concurrently, surface nitrate started to decrease and was very low during the  
329 stratification period, from May to October (mean concentration in the top 20 m of 0.28  
330  $\mu\text{mol kg}^{-1}$ ). This caused the formation of a marked nitracline at ~ 40 m depth (Figs. 2a  
331 and 3c).

332 In contrast to nitrate, Chl a exhibited higher concentrations in near-surface waters  
333 except in mid-winter, when mixing homogenized the water column, and in mid-summer  
334 when the chlorophyll maximum was observed close to the depth of the nitracline (Fig.  
335 3d). Depth-integrated Chl a increased markedly in late December (Fig. 3f), although

336 surface concentrations only increased in late February with the onset of stratification  
337 (Figs. 3d and 3h). This fast increase in Chl a corresponds to the spring bloom and accounts  
338 for most of the seasonal depletion of near-surface nitrate. It represents the annual  
339 maximum in phytoplankton biomass, which generally occurred in March near-surface  
340 (Figs. 3d, 3h and 4) and ranged from 0.23 to 5.41 mg m<sup>-3</sup> (average Chl a concentration in  
341 the uppermost 20 m). The annual maximum decreased in magnitude with depth and  
342 occurred later at intermediate-depth waters from 30 to 50 m (Fig. 4). From June to  
343 September, Chl a concentrations remained low near-surface (Figs. 3d and 3h) with the  
344 maximum observed between 20 and 50 m (0.33 mg m<sup>-3</sup> on average). Surface Chl a  
345 concentration increased again during the autumn bloom, which usually peaked in  
346 November (Fig. 3d and 3h) and was weaker than the spring bloom (average Chl a  
347 concentration of 0.18-2.64 mg m<sup>-3</sup> in the uppermost 20 m).

#### 348 **Effect of WMD<sub>max</sub> on the vertical structure of the spring bloom**

349 Maximum winter mixing depths (WMD<sub>max</sub>) exhibited inter-annual variability in both  
350 magnitude and timing (Fig. 5a). This variability affected the nutrient supply to surface  
351 layers: the deeper the WMD<sub>max</sub>, the larger the depth-integrated nitrate over the upper 50  
352 m (Figs. 5b and 5c). Winter mixing also affected nitrate levels and Chl a in spring blooms,  
353 as seen in Table 1. Data for March were used to analyze this effect, the month in which  
354 the near-surface spring bloom typically peaks (Figs. 3d, 3h and 4). The model that  
355 includes WMD<sub>max</sub> and MLD<sub>0.1</sub> as predictors of nitrate and Chl a concentrations performed  
356 best (Table 1). This indicates that both the past and recent history of water-column  
357 stratification (i.e. WMD<sub>max</sub> and MLD<sub>0.1</sub>, respectively) have an effect on nitrate and Chl a  
358 concentrations during the spring bloom. This model shows that higher nitrate and Chl a  
359 concentrations in March follow winters with deeper WMD<sub>max</sub> (left panels in Fig. 6). The

This is the accepted version of the following article: González-Gil, R., González Taboada, F., Cáceres, C., Largier, J. L. and Anadón, R. (2017), Winter-mixing preconditioning of the spring phytoplankton bloom in the Bay of Biscay. *Limnol. Oceanogr.* doi:10.1002/lno.10769, which has been published in final form at [Limnology & Oceanography](#). This article may be used for non-commercial purposes in accordance with the [Wiley Self-Archiving Policy](#).

360 positive effect of  $WMD_{max}$  on nitrate concentration was more important towards the  
361 surface (i.e., the increase in the effect along the x axis is gradually larger towards  
362 shallower depths in the left panel of Fig. 6a). A similar effect was found for Chl a; the  
363 positive effect of  $WMD_{max}$  was also strongest in surface waters and it became weaker at  
364 deeper depths, especially at intermediate layers (left panel in Fig. 6b). In both cases, the  
365 near-surface seasonal depletion of nutrients during stratification (Figs. 3c, 3e and 3g) can  
366 explain the higher near-surface sensitivity of nitrate and Chl a to winter mixing.

367 Contrary to the effect of  $WMD_{max}$ , the relationship between near-surface stratification  
368 depth ( $MLD_{0.1}$ ) and either nitrate or Chl a concentrations in March varied markedly across  
369 depth (right panels in Fig. 6). In the case of nitrate, near-surface concentrations decrease  
370 when  $MLD_{0.1}$  is shallow ( $MLD_{0.1} \sim 0$  to 75 m, right panel of Fig. 6a), with strongest  
371 decreases for shallowest  $MLD_{0.1}$ . This effect of  $MLD_{0.1}$  on nitrate is consistent with rapid  
372 nutrient drawdown when phytoplankton blooms are confined within a thin surface layer  
373 (depth given by  $MLD_{0.1}$ ). Consistent with this forcing, large Chl a concentrations are seen  
374 near-surface and at depth (below  $\sim 150$  m) when  $MLD_{0.1}$  is less than  $\sim 100$  m (see right  
375 panel of Fig. 6b). The effect in other sections of the water column (below  $\sim 50$  m for  
376 nitrate, but  $\sim 30$ -150 m for Chl a) peaked at intermediate  $MLD_{0.1}$  ( $\sim 50$ -125 m).

377 Table 2 summarizes the effect of  $WMD_{max}$  and  $MLD_{0.1}$  on surface nitrate and Chl a  
378 concentrations in March. In the case of nitrate, the model including only  $MLD_{0.1}$   
379 explained around three times more variability than the  $WMD_{max}$  alone (Table 2); the  
380 model including an interaction showed a positive effect of  $MLD_{0.1}$ , which was similar  
381 along the entire  $WMD_{max}$  range, and a decreasing positive effect of  $WMD_{max}$  towards  
382 deeper  $MLD_{0.1}$  (Fig. 7a). In the case of Chl a, the interaction model outcompeted the  
383 others (Table 2). For the analysis of the model outputs portrayed in Fig. 7b, we focused

384 on those regions of the sample space with observations. Surface Chl a concentration was  
385 maximum for deep  $WMD_{max}$  and shallow  $MLD_{0.1}$  and showed a secondary maximum for  
386  $MLD_{0.1} \sim 50-100$  m. Depth-integrated Chl a in March, which was highly correlated with  
387 Chl a at 20-30 m depth (Supporting information Fig. S1a), showed a similar response  
388 pattern as surface Chl a. However, maximum depth-integrated Chl a showed  
389 approximately the same values for  $MLD_{0.1} \sim 50-150$  m as for deep  $WMD_{max}$  and shallow  
390  $MLD_{0.1}$  (Fig. S1b).

391 The new primary production ( $PP_{new}$ ) during the spring bloom, estimated from depth-  
392 integrated nitrate (0-50 m) depletion, was between 30 and 490  $mg\ C\ m^{-2}\ day^{-1}$  (Fig. 8).  
393 We found a clear relationship between primary production and  $WMD_{max}$  ( $R^2 = 0.41$ , p-  
394 value = 0.026). This model predicts an increase in  $PP_{new}$  of  $\sim 64\ mg\ C\ m^{-2}\ day^{-1}$  for every  
395 100 m increase in  $WMD_{max}$ .

397 High-resolution satellite data allowed characterization of the development of the  
398 spring phytoplankton bloom at the surface. Spring bloom phenology exhibited high  
399 interannual variability (Fig. 9), typically lasting ~ 90 days and peaking between February  
400 17<sup>th</sup> and May 22<sup>nd</sup> (with mean date of April 4<sup>th</sup>). The magnitude of the bloom also varied  
401 between years, with [Chl a]<sub>SAT</sub> peak concentrations ranging from 0.53 to 1.43 mg m<sup>-3</sup>.  
402 Changes in bloom magnitude were positively associated with WMD<sub>max</sub> (Fig. 10e),  
403 consistent with the analysis of in situ data. Later blooms with a shorter span followed  
404 winters with deeper mixing layers (Figs. 10a and 10i), although the effect of WMD<sub>max</sub> on  
405 these timing metrics remained more elusive ( $R^2 = 0.15$ , p-value = 0.165 for bloom rise;  
406  $R^2 = 0.18$ , p-value = 0.133 for bloom span). As mentioned above, the bloom was more  
407 productive in years with deep WMD<sub>max</sub> (Fig. 8). Additionally, the later the WMD<sub>max</sub>  
408 occurred, the later the spring bloom peaked (Fig. 10h). A simple linear correlation  
409 analysis showed that WMD<sub>max</sub> and the WMD<sub>max</sub> sampling day were uncorrelated ( $r =$   
410 0.30, p-value = 0.302).

411

**Impact of SST on WMD<sub>max</sub>**

412 The WMD<sub>max</sub> was negatively correlated with the SST, indicating that shallower  
413 WMD<sub>max</sub> follow warmer SST (Fig. 11a). These negative relationships were stronger for  
414 SST within ~ 60 days prior to the winter mixing event. Thus the December-March SST  
415 is most important in accounting for WMD<sub>max</sub>, which mostly occurred in February and  
416 March (Fig. 5a). On the other hand, the SST seasonal cycle exhibited large interannual  
417 variation (Fig. 9). Beyond the observed linear trend (0.30 °C decade<sup>-1</sup>, 1981-2012), this  
418 variation reflects different rates of warming through the year, with largest values observed

419 during the period of seasonal stratification (spring to early autumn), when the trend  
420 frequently exceeds  $0.30\text{ }^{\circ}\text{C decade}^{-1}$  (Fig. 11b). This positive trend in SST indicates a  
421 long-term decline in  $\text{WMD}_{\text{max}}$  and consequently in the magnitude of the spring bloom  
422 (see Fig. 10e). However, the short length of the record prevented a direct assessment of  
423 these trends and further exploration of this link is required.

## 424 **Discussion**

425 Our results demonstrate a strong winter-mixing preconditioning of the development  
426 and characteristics of the spring phytoplankton bloom, modulated by near-surface  
427 stratification. Deeper and later winter mixing leads to more intense and later spring  
428 blooms. These more intense blooms are also more productive, as indicated by the faster  
429 nitrate decrease in near-surface waters. Additionally, we found that higher winter SST is  
430 associated with weaker mixing in winter, and thus also associated with weaker spring  
431 phytoplankton blooms.

432 The dynamics of the spring phytoplankton bloom remain a subject of active debate  
433 among marine scientists (see Behrenfeld and Boss 2014; Chiswell et al. 2015 for recent  
434 reviews). Some of this controversy arises from the adoption of different methods to  
435 characterize phytoplankton blooms (Ji et al. 2010), with contrasting findings depending  
436 on whether the analyses focused on surface or depth-integrated phytoplankton biomass  
437 (Chiswell et al. 2015). Nevertheless, both approaches disregard the depth-dependence of  
438 the phytoplankton response, which we describe here and that accounts for observed  
439 differences in timing and magnitude of the spring bloom.

440 The spring bloom exhibits yearly an apparent northward and southward progression in  
441 the Northern and Southern Hemisphere, respectively (Siegel et al. 2002; Henson et al.  
442 2009; Chiswell et al. 2013). Analogously, in the Bay of Biscay and presumably also in  
443 other temperate regions (see for example Chiswell 2011), the spring bloom exhibits an  
444 apparent progression into subsurface layers as spring progresses and the water column  
445 stratifies. For upper layers, we understand this in terms of changes in the optimal nutrient  
446 and light conditions for phytoplankton growth (Klausmeier and Litchman 2001). In deep



447 layers, the seasonal timing of maximum Chl a might reflect a larger arrival of  
448 phytoplankton cells from near-surface waters and positive phytoplankton growth during  
449 winter, potentially due to a dilution effect on grazing (Behrenfeld 2010; Behrenfeld 2014;  
450 Behrenfeld and Boss 2014). The observed seasonal increase in depth-integrated  
451 phytoplankton biomass during winter supports this last aspect to some extent, but our  
452 confidence is constrained by limited data availability during winter.

453 The observed seasonal cycle of Chl a in the Bay of Biscay shows that the development  
454 of the spring bloom in surface waters occurs in March. A shift from a deep-mixing regime  
455 (primarily buoyancy-driven) to a low-turbulence regime (mainly wind-driven) occurs  
456 during this critical period (Huisman et al. 1999; Chiswell et al. 2013; Brody and Lozier  
457 2014; 2015; Chiswell et al. 2015). This period coincides also with the onset of the  
458 seasonal thermal stratification, triggered by a change to positive air-sea heat fluxes  
459 (Chiswell 2011; Taylor and Ferrari 2011; Ferrari et al. 2015). Nitrate concentration at the  
460 beginning of the spring bloom is largely controlled by the magnitude of deep mixing  
461 events in the prior winter, as already shown by Hartman et al. (2013). However, inter-  
462 annual changes in the characteristics of upper water masses and different hydrographic  
463 processes (e.g. the Iberian Poleward Current, IPC) can modulate the effect of winter  
464 mixing on nutrient preconditioning (Llope et al. 2007).

465 Winter convective mixing increases near-surface nutrient concentration directly  
466 through nutrient entrainment from deep waters (Mann and Lazier 2006; Sarmiento and  
467 Gruber 2006). Additionally, it reduces the time spent by phytoplankton in the euphotic  
468 layer, lowering population growth rates (Sverdrup 1953), and also diluting phytoplankton  
469 concentrations (Evans and Parslow 1985; Backhaus et al. 2003; D'Asaro 2008). Both  
470 processes reduce nutrient uptake by phytoplankton in the upper ocean. However, this

471 dilution through mixing also reduces encounter rates with potential grazers, lowering the  
472 grazing pressure on phytoplankton population in winter (Yoshie et al. 2003; Behrenfeld  
473 2010; Behrenfeld and Boss 2014). Combining the arguments presented above, deeper  
474 winter mixing can lead to a high-nutrient, low-grazing environment that may positively  
475 precondition phytoplankton growth during the spring bloom. Indeed, our analysis  
476 demonstrates that deeper winter mixing is associated with higher nutrient concentrations  
477 and more intense blooms in the southern Bay of Biscay.

478 The physical structure of the water column during the spring bloom, characterized by  
479 near-surface stratification, plays also an important role in shaping the vertical distribution  
480 of phytoplankton (Chiswell 2011; Brody and Lozier 2015). The thickness of the stratified  
481 layer determines how far phytoplankton can be moved downward, away from maximum  
482 light intensities (Franks 2015). Shoaling stratification in March keeps phytoplankton  
483 closer to the surface and exposed to higher aggregate light, leading to an increase in their  
484 growth rates (Chiswell 2011), and rapid removal of nitrate from these surface waters. We  
485 observed that surface phytoplankton biomass was enhanced by shallow-intermediate  
486 stratified layers, especially after a favorable preconditioning by mid-large winter mixing  
487 events. Higher Chl a concentrations at depth during shallow-intermediate stratification  
488 and after mid-large winter mixing may be due to larger fluxes of sinking cells due to  
489 enhanced phytoplankton growth in the upper layers (Falkowski et al. 1998; Sanders et al.  
490 2014). In temperate seas such as the Bay of Biscay, diatoms become the dominant  
491 phytoplankton group during the spring bloom (Fernández and Bode 1994) and their  
492 sinking rates can be greater than  $100 \text{ m d}^{-1}$ , enhanced by particle aggregation (Smayda  
493 1970; Lampitt 1985; Smetacek 1985; Burd and Jackson 2009). Thus, increased diatom  
494 growth in the surface during the bloom might lead to a rapid export of phytoplankton to

495 waters several hundreds of meters below. In our study area, this hypothesis is supported  
496 by the large pulses of biogenic silica collected by deep sediment traps during the spring  
497 blooms of 2012 and 2013 (Rumín-Caparrós et al. 2016; traps were moored at 1178 and  
498 1154 m depth over the Avilés Canyon and westwards over the open slope, respectively).

499 Winter-mixing preconditioning also affected different metrics of the spring bloom in  
500 the surface layer. As observed in March for in situ Chl a concentrations, the high nutrient  
501 environment caused by deeper winter mixing events was associated with larger spring  
502 bloom peaks. This positive effect of deep convective mixing on the spring bloom has  
503 been observed in other areas of the North Atlantic (Martinez et al. 2011; Behrenfeld et al.  
504 2013). However, our results demonstrate that enhanced nitrate concentrations following  
505 strong winter mixing also lead to a more rapid uptake of nutrients in spring. This rapid  
506 consumption reflects a larger accumulation of phytoplankton biomass and results in a  
507 shorter but more intense bloom. In this way, deeper mixing leads to higher community  
508 productivity in the Bay of Biscay (Hartman et al. 2013) and larger peaks in spring  
509 zooplankton biomass and abundance (González-Gil et al. 2015). This bottom-up  
510 perspective is also compatible with top-down mechanisms raised in the context of the  
511 Dilution-Recoupling Hypothesis (Behrenfeld 2010). The release of phytoplankton from  
512 grazing pressure in winters with enhanced mixing could entail the development of a larger  
513 seeding population and a bloom of a greater magnitude. Interestingly, a lower grazing  
514 rate could also reduce in situ nutrient regeneration and foster nutrient consumption by  
515 enabling higher accumulations of phytoplankton biomass (Banse 1992), with the overall  
516 result of more intense blooms with a shortened span.

517 Strong surface cooling processes due to heat losses are one of the major drivers of deep  
518 convective events in winter, as observed in 2005 in the Bay of Biscay (Somavilla et al.

519 2009; Acuña et al. 2010; Somavilla Cabrillo et al. 2011). Also, intense winds related to  
520 winter storms may contribute to stirring of the water column during deep mixing (Henson  
521 et al. 2006). If any or both of these processes occur at the end of winter, they could delay  
522 the beginning of thermal stratification or break it temporarily during its initial phase.  
523 Thermal stratification of the water column is required for full development of the near-  
524 surface spring bloom (Chiswell 2011; Chiswell et al. 2015). Thus, later deep mixing  
525 events associated with lower atmospheric temperatures and gales at the end of winter  
526 would delay the spring bloom climax (Townsend et al. 1994; Henson et al. 2006; Álvarez  
527 et al. 2009). This could explain our observation that later deep winter mixing events  
528 caused later spring bloom peaks.

529 The trend towards surface warming in the southern Bay of Biscay in winter is  
530 consistent with both observational and model-based increases in heat content in North  
531 Atlantic surface waters (Danabasoglu et al. 2012; Taboada and Anadón 2012). A larger  
532 increase in surface heat content relative to deeper layers represents increasing stability  
533 and the need for larger energy inputs to mix the water column (Levitus et al. 2012). The  
534 presumed decay in winter mixing associated with warming surface waters can be  
535 expected to cause a decline in the magnitude of the spring phytoplankton bloom in the  
536 Cantabrian Sea. Less intense blooms would decrease the strength of the biological pump  
537 (Falkowski et al. 1998; Sanders et al. 2014), and they can also lead to a trophic mismatch  
538 and a decrease in the production of upper trophic levels (Durant et al. 2007). Nevertheless,  
539 the short length of the series analyzed in this study recommends caution in interpreting  
540 trend results (e.g. Henson et al. 2010).

541 The impact of large-scale climate patterns such as the North Atlantic Oscillation  
542 (NAO, Hurrell and Deser 2009) deters a simple interpretation of the long-term variability

543 in the Bay of Biscay associated with climate change. Indeed, changes in the intensity of  
544 winter mixing have been linked to changes in atmospheric circulation and air-sea heat  
545 fluxes in the Bay of Biscay associated with alternating phases of the NAO (Somavilla  
546 Cabrillo et al. 2011). Positive NAO promotes surface warming and shallower mixing in  
547 winter. However, extremely deep winter mixing events were common following a  
548 decade-long switch in NAO state starting in the mid-1990s. These strong winter mixing  
549 events are also associated with negative anomalies of the East Atlantic (EA) pattern that  
550 bring cold, northerly winds into the southern Bay of Biscay (Somavilla et al. 2009).  
551 Although continued warming might eventually conceal these effects, the consequences  
552 of changes in winter mixing, spring stratification and the interaction with long-term  
553 forcing remains elusive. Together, our findings recommend a continued monitoring and  
554 further analysis of potential changes in plankton phenology in the Bay of Biscay.

## 555        **Conclusions**

556        Deep winter-mixing preconditioning affects nitrate and Chl a concentrations during  
557        the spring phytoplankton bloom in oceanic waters of the southern Bay of Biscay. Deeper  
558        winter mixing enhances phytoplankton biomass and nitrate concentrations during spring  
559        through the entire water column. On shorter time scales, the physical structure of the  
560        water column, characterized by the depth of the surface stratified layer, had an important  
561        role in shaping the vertical profiles of nitrate and phytoplankton. Our results show that  
562        deeper and later winter mixing events led to later and more intense spring blooms. The  
563        faster rate of nitrate uptake during this type of bloom indicates enhanced primary  
564        production. Finally, we found that warm surface temperatures, especially in winter, were  
565        associated with weaker mixing of the water column and consequently, with a smaller  
566        spring bloom peak. Observations and predictions of increasing surface temperature in  
567        winter thus suggest a potential weakening of the spring bloom and a reduction of upper  
568        trophic productivity and deep carbon export in the Bay of Biscay. This might also be  
569        observed in other temperate areas in the future.

570       **References**

- 571       Acuña, J. L., M. López-Alvarez, E. Nogueira, and F. González-Taboada. 2010. Diatom  
572       flotation at the onset of the spring phytoplankton bloom: an in situ experiment.  
573       *Mar. Ecol. Prog. Ser.* **400**: 115-125. doi:10.3354/meps08405
- 574       Álvarez, E., E. Nogueira, J. L. Acuña, M. López-Álvarez, and J. A. Sostres. 2009. Short-  
575       term dynamics of late-winter phytoplankton blooms in a temperate ecosystem  
576       (Central Cantabrian Sea, Southern Bay of Biscay). *J. Plankton Res.* **31**: 601-617.  
577       doi:10.1093/plankt/fbp012
- 578       Backhaus, J. O., E. N. Hegseth, H. Wehde, X. Irigoien, K. Hatten, and K. Logemann.  
579       2003. Convection and primary production in winter. *Mar. Ecol. Prog. Ser.* **251**: 1-  
580       14. doi:10.3354/meps251001
- 581       Banse, K. 1992. Grazing, temporal changes of phytoplankton concentrations, and the  
582       microbial loop in the open sea, p. 409-440. In P. G. Falkowski and A. D.  
583       Woodhead [eds.], *Primary productivity and biogeochemical cycles in the sea*.  
584       Plenum Press.
- 585       Behrenfeld, M. J. 2010. Abandoning Sverdrup's critical depth hypothesis on  
586       phytoplankton blooms. *Ecology* **91**: 977-989. doi:10.1890/09-1207.1
- 587       Behrenfeld, M. J. 2014. Climate-mediated dance of the plankton. *Nat. Clim. Change* **4**:  
588       880-887. doi:10.1038/nclimate2349
- 589       Behrenfeld, M. J., and E. S. Boss. 2014. Resurrecting the ecological underpinnings of  
590       ocean plankton blooms. *Annu. Rev. Mar. Sci.* **6**: 167-194. doi:10.1146/annurev-  
591       marine-052913-021325
- 592       Behrenfeld, M. J., S. C. Doney, I. Lima, E. S. Boss, and D. A. Siegel. 2013. Annual cycles  
593       of ecological disturbance and recovery underlying the subarctic Atlantic spring  
594       plankton bloom. *Glob. Biogeochem. Cycles* **27**: 526-540. doi:10.1002/gbc.20050
- 595       Blondeau-Patissier, D., J. F. R. Gower, A. G. Dekker, S. R. Phinn, and V. E. Brando.  
596       2014. A review of ocean color remote sensing methods and statistical techniques  
597       for the detection, mapping and analysis of phytoplankton blooms in coastal and  
598       open oceans. *Prog. Oceanogr.* **123**: 123-144. doi:10.1016/j.pocean.2013.12.008
- 599       Brody, S. R., and M. S. Lozier. 2014. Changes in dominant mixing length scales as a  
600       driver of subpolar phytoplankton bloom initiation in the North Atlantic. *Geophys.*  
601       *Res. Lett.* **41**: 3197-3203. doi:10.1002/2014GL059707
- 602       Brody, S. R., and M. S. Lozier. 2015. Characterizing upper-ocean mixing and its effect  
603       on the spring phytoplankton bloom with in situ data. *ICES J. Mar. Sci.* **72**: 1961-  
604       1970. doi:10.1093/icesjms/fsv006
- 605       Brody, S. R., M. S. Lozier, and J. P. Dunne. 2013. A comparison of methods to determine  
606       phytoplankton bloom initiation. *J. Geophys. Res.: Oceans* **118**: 2345-2357.  
607       doi:10.1002/jgrc.20167

This is the accepted version of the following article: González-Gil, R., González Taboada, F., Cáceres, C., Largier, J. L. and Anadón, R. (2017), Winter-mixing preconditioning of the spring phytoplankton bloom in the Bay of Biscay. *Limnol. Oceanogr.* doi:10.1002/lno.10769, which has been published in final form at [Limnology & Oceanography](https://doi.org/10.1002/lno.10769). This article may be used for non-commercial purposes in accordance with the [Wiley Self-Archiving Policy](https://doi.org/10.1002/lno.10769).

- 608 Burd, A. B., and G. A. Jackson. 2009. Particle aggregation. *Annu. Rev. Mar. Sci.* **1**: 65-  
609 90. doi:10.1146/annurev.marine.010908.163904
- 610 Burnham, K. P., and D. R. Anderson. 2002. Model selection and multimodel inference: a  
611 practical information-theoretic approach. Springer-Verlag.
- 612 Cullen, J., and R. Eppley. 1981. Chlorophyll maximum layers of the Southern California  
613 Bight and possible mechanisms of their formation and maintenance. *Oceanol.*  
614 *Acta* **4**: 23-32. <http://archimer.ifremer.fr/doc/00121/23207/>.
- 615 Cushing, D. 1990. Plankton production and year-class strength in fish populations: an  
616 update of the match/mismatch hypothesis. *Adv. Mar. Biol.* **26**: 249-293.  
617 doi:10.1016/S0065-2881(08)60202-3
- 618 Chiswell, S. M. 2011. Annual cycles and spring blooms in phytoplankton: don't abandon  
619 Sverdrup completely. *Mar. Ecol. Prog. Ser.* **443**: 39-50. doi:10.3354/meps09453
- 620 Chiswell, S. M., J. Bradford-Grieve, M. G. Hadfield, and S. C. Kennan. 2013.  
621 Climatology of surface chlorophyll a, autumn-winter and spring blooms in the  
622 southwest Pacific Ocean. *J. Geophys. Res.: Oceans* **118**: 1003-1018.  
623 doi:10.1002/jgrc.20088
- 624 Chiswell, S. M., P. H. R. Calil, and P. W. Boyd. 2015. Spring blooms and annual cycles  
625 of phytoplankton: a unified perspective. *J. Plankton Res.* **37**: 500-508.  
626 doi:10.1093/plankt/fbv021
- 627 Church, M. J., M. W. Lomas, and F. Muller-Karger. 2013. Sea change: Charting the  
628 course for biogeochemical ocean time-series research in a new millennium. *Deep*  
629 *Sea Res. Part II* **93**: 2-15. doi:10.1016/j.dsr2.2013.01.035
- 630 D'Asaro, E. A. 2008. Convection and the seeding of the North Atlantic bloom. *J. Mar.*  
631 *Syst.* **69**: 233-237. doi:10.1016/j.jmarsys.2005.08.005
- 632 D'Ortenzio, F. and others. 2014. Observing mixed layer depth, nitrate and chlorophyll  
633 concentrations in the northwestern Mediterranean: A combined satellite and NO3  
634 profiling floats experiment. *Geophys. Res. Lett.* **41**: 6443-6451.  
635 doi:10.1002/2014GL061020
- 636 Danabasoglu, G., S. C. Bates, B. P. Briegleb, S. R. Jayne, M. Jochum, W. G. Large, S.  
637 Peacock, and S. G. Yeager. 2012. The CCSM4 ocean component. *J. Clim.* **25**:  
638 1361-1389. doi:10.1175/JCLI-D-11-00091.1
- 639 Dever, E. P., C. E. Dorman, and J. L. Largier. 2006. Surface boundary-layer variability  
640 off Northern California, USA, during upwelling. *Deep Sea Res. Part II* **53**: 2887-  
641 2905. doi:10.1016/j.dsr2.2006.09.001
- 642 Durant, J. M., D. Ø. Hjermann, G. Ottersen, and N. C. Stenseth. 2007. Climate and the  
643 match or mismatch between predator requirements and resource availability.  
644 *Clim. Res.* **33**: 271-283. doi:10.3354/cr033271



- 645 Eppley, R. W. 1972. Temperature and phytoplankton growth in the sea. *Fish. Bull.* **70**:  
646 1063-1085.
- 647 Evans, G. T., and J. S. Parslow. 1985. A Model of Annual Plankton Cycles. *Biological*  
648 *Oceanography* **3**: 327-347. doi:10.1080/01965581.1985.10749478
- 649 Falkowski, P. G., R. T. Barber, and V. Smetacek. 1998. Biogeochemical controls and  
650 feedbacks on ocean primary production. *Science* **281**: 200-206.  
651 doi:10.1126/science.281.5374.200
- 652 Fernández, E., and A. Bode. 1994. Succession of phytoplankton assemblages in relation  
653 to the hydrography in the southern Bay of Biscay: a multivariate approach. *Sci.*  
654 *Mar.* **58**: 191-205.  
655 <http://www.icm.csic.es/scimar/index.php/secId/196/IdArt/2688/>.
- 656 Ferrari, R., S. T. Merrifield, and J. R. Taylor. 2015. Shutdown of convection triggers  
657 increase of surface chlorophyll. *J. Mar. Syst.* **147**: 116-122.  
658 doi:10.1016/j.jmarsys.2014.02.009
- 659 Ferreira, A. S. A., H. Hátún, F. Counillon, M. R. Payne, and A. W. Visser. 2015.  
660 Synoptic-scale analysis of mechanisms driving surface chlorophyll dynamics in  
661 the North Atlantic. *Biogeosciences* **12**: 3641-3653. doi:10.5194/bg-12-3641-2015
- 662 Fischer, A., E. Moberg, H. Alexander, E. Brownlee, K. Hunter-Cevera, K. Pitz, S.  
663 Rosengard, and H. Sosik. 2014. Sixty years of Sverdrup: a retrospective of  
664 progress in the study of phytoplankton blooms. *Oceanography* **27**: 222-235.  
665 doi:10.5670/oceanog.2014.26
- 666 Follows, M., and S. Dutkiewicz. 2002. Meteorological modulation of the North Atlantic  
667 spring bloom. *Deep Sea Res. Part II* **49**: 321-344. doi:10.1016/S0967-  
668 0645(01)00105-9
- 669 Franks, P. J. S. 2015. Has Sverdrup's critical depth hypothesis been tested? Mixed layers  
670 vs. turbulent layers. *ICES J. Mar. Sci.* **72**: 1897-1907. doi:10.1093/icesjms/fsu175
- 671 González-Gil, R., F. G. Taboada, J. Höfer, and R. Anadón. 2015. Winter mixing and  
672 coastal upwelling drive long-term changes in zooplankton in the Bay of Biscay  
673 (1993–2010). *J. Plankton Res.* **37**: 337-351. doi:10.1093/plankt/fbv001
- 674 González Taboada, F., and R. Anadón. 2014. Seasonality of North Atlantic phytoplankton  
675 from space: impact of environmental forcing on a changing phenology (1998–  
676 2012). *Glob. Change Biol.* **20**: 698-712. doi:10.1111/gcb.12352
- 677 Hartman, S. E., M. C. Hartman, D. J. Hydes, Z.-P. Jiang, D. Smythe-Wright, and C.  
678 González-Pola. 2013. Seasonal and inter-annual variability in nutrient supply in  
679 relation to mixing in the Bay of Biscay. *Deep Sea Res. Part II* **57**: 1303-1312.  
680 doi:10.1016/j.dsr2.2013.09.032
- 681 Hastie, T. J., and R. J. Tibshirani. 1990. Generalized additive models. Chapman &  
682 Hall/CRC.

This is the accepted version of the following article: González-Gil, R., González Taboada, F., Cáceres, C., Largier, J. L. and Anadón, R. (2017), Winter-mixing preconditioning of the spring phytoplankton bloom in the Bay of Biscay. *Limnol. Oceanogr.* doi:10.1002/lno.10769, which has been published in final form at [Limnology & Oceanography](#). This article may be used for non-commercial purposes in accordance with the [Wiley Self-Archiving Policy](#).

- 683 Henson, S. A., J. P. Dunne, and J. L. Sarmiento. 2009. Decadal variability in North  
684 Atlantic phytoplankton blooms. *J. Geophys. Res.: Oceans* **114**: C04013.  
685 doi:10.1029/2008JC005139
- 686 Henson, S. A., I. Robinson, J. T. Allen, and J. J. Waniek. 2006. Effect of meteorological  
687 conditions on interannual variability in timing and magnitude of the spring bloom  
688 in the Irminger Basin, North Atlantic. *Deep Sea Res. Part I* **53**: 1601-1615.  
689 doi:10.1016/j.dsr.2006.07.009
- 690 Henson, S. A., J. L. Sarmiento, J. P. Dunne, L. Bopp, I. Lima, S. C. Doney, J. John, and  
691 C. Beaulieu. 2010. Detection of anthropogenic climate change in satellite records  
692 of ocean chlorophyll and productivity. *Biogeosciences* **7**: 621-640.  
693 doi:10.5194/bg-7-621-2010
- 694 Hjort, J. 1914. Fluctuations in the great fisheries of northern Europe viewed in the light  
695 of biological research. *Rapp. P.-V. Reün. Cons. Intern. Explor. Mer.* **20**: 1-228.
- 696 Houpert, L., P. Testor, X. D. de Madron, S. Somot, F. D'Ortenzio, C. Estournel, and H.  
697 Lavigne. 2015. Seasonal cycle of the mixed layer, the seasonal thermocline and  
698 the upper-ocean heat storage rate in the Mediterranean Sea derived from  
699 observations. *Prog. Oceanogr.* **132**: 333-352. doi:10.1016/j.pocean.2014.11.004
- 700 Huisman, J., P. van Oostveen, and F. J. Weissing. 1999. Critical depth and critical  
701 turbulence: two different mechanisms for the development of phytoplankton  
702 blooms. *Limnol. Oceanogr.* **44**: 1781-1787. doi:10.4319/lo.1999.44.7.1781
- 703 Hurrell, J. W., and C. Deser. 2009. North Atlantic climate variability: The role of the  
704 North Atlantic Oscillation. *J. Mar. Syst.* **78**: 28-41.  
705 doi:10.1016/j.jmarsys.2008.11.026
- 706 Ikeda, T. 1985. Metabolic rates of epipelagic marine zooplankton as a function of body  
707 mass and temperature. *Mar. Biol.* **85**: 1-11. doi:10.1007/BF00396409
- 708 Ji, R., M. Edwards, D. L. Mackas, J. A. Runge, and A. C. Thomas. 2010. Marine plankton  
709 phenology and life history in a changing climate: current research and future  
710 directions. *J. Plankton Res.* **32**: 1355-1368. doi:10.1093/plankt/fbq062
- 711 Karl, D. M. 2010. Oceanic ecosystem time-series programs: Ten lessons learned.  
712 *Oceanography* **23**: 104-125. doi:10.5670/oceanog.2010.27
- 713 Klausmeier, C. A., and E. Litchman. 2001. Algal games: The vertical distribution of  
714 phytoplankton in poorly mixed water columns. *Limnol. Oceanogr.* **46**: 1998-  
715 2007. doi:10.4319/lo.2001.46.8.1998
- 716 Koeller, P. and others. 2009. Basin-scale coherence in phenology of shrimps and  
717 phytoplankton in the North Atlantic Ocean. *Science* **324**: 791-793.  
718 doi:10.1126/science.1170987
- 719 Körtzinger, A., W. Koeve, P. Kähler, and L. Mintrop. 2001. C : N ratios in the mixed  
720 layer during the productive season in the northeast Atlantic Ocean. *Deep Sea Res.*  
721 *Part I* **48**: 661-688. doi:https://doi.org/10.1016/S0967-0637(00)00051-0

This is the accepted version of the following article: González-Gil, R., González Taboada, F., Cáceres, C., Largier, J. L. and Anadón, R. (2017), Winter-mixing preconditioning of the spring phytoplankton bloom in the Bay of Biscay. *Limnol. Oceanogr.* doi:10.1002/lno.10769, which has been published in final form at [Limnology & Oceanography](https://doi.org/10.1002/lno.10769). This article may be used for non-commercial purposes in accordance with the [Wiley Self-Archiving Policy](https://doi.org/10.1002/lno.10769).

- 722 Kristiansen, T., K. F. Drinkwater, R. G. Lough, and S. Sundby. 2011. Recruitment  
723 variability in North Atlantic cod and match-mismatch dynamics. *PLoS One* **6**:  
724 e17456. doi:10.1371/journal.pone.0017456
- 725 Lampitt, R. S. 1985. Evidence for the seasonal deposition of detritus to the deep-sea floor  
726 and its subsequent resuspension. *Deep-Sea Res. Part A Oceanogr. Res. Pap.* **32**:  
727 885-897. doi:10.1016/0198-0149(85)90034-2
- 728 Levitus, S. and others. 2012. World ocean heat content and thermosteric sea level change  
729 (0–2000 m), 1955–2010. *Geophys. Res. Lett.* **39**: L10603.  
730 doi:10.1029/2012GL051106
- 731 Lindemann, C., and M. A. St. John. 2014. A seasonal diary of phytoplankton in the North  
732 Atlantic. *Front. Mar. Sci.* **1**: 1-6. doi:10.3389/fmars.2014.00037
- 733 Longhurst, A. R., and W. G. Harrison. 1989. The biological pump: profiles of plankton  
734 production and consumption in the upper ocean. *Prog. Oceanogr.* **22**: 47-123.  
735 doi:10.1016/0079-6611(89)90010-4
- 736 Llope, M., R. Anadón, J. Á. Sostres, and L. Viesca. 2007. Nutrients dynamics in the  
737 southern Bay of Biscay (1993–2003): winter supply, stoichiometry, long-term  
738 trends, and their effects on the phytoplankton community. *J. Geophys. Res.:*  
739 *Oceans* **112**: C07029. doi:10.1029/2006JC003573
- 740 Llope, M., R. Anadón, L. Viesca, M. Quevedo, R. González-Quirós, and N. C. Stenseth.  
741 2006. Hydrography of the southern Bay of Biscay shelf-break region: integrating  
742 the multiscale physical variability over the period 1993-2003. *J. Geophys. Res.:*  
743 *Oceans* **111**: C09021. doi:10.1029/2005JC002963
- 744 Mann, K. H., and J. R. N. Lazier. 2006. Dynamics of marine ecosystems. *Biological–*  
745 *Physical Interactions in the Oceans*, 3rd ed. Blackwell.
- 746 Martinez, E., D. Antoine, F. D'Ortenzio, and C. de Boyer Montégut. 2011. Phytoplankton  
747 spring and fall blooms in the North Atlantic in the 1980s and 2000s. *J. Geophys.*  
748 *Res.: Oceans* **116**: C11029. doi:10.1029/2010JC006836
- 749 McClain, C. R. 2009. A decade of satellite ocean color observations. *Annu. Rev. Mar.*  
750 *Sci.* **1**: 19-42. doi:10.1146/annurev.marine.010908.163650
- 751 Monterey, G. I., and S. Levitus. 1997. Seasonal variability of mixed layer depth for the  
752 World Ocean. NOAA Atlas NESDIS 14, US Government Printing Office.
- 753 Moore, C. M. and others. 2013. Processes and patterns of oceanic nutrient limitation. *Nat.*  
754 *Geosci.* **6**: 701-710. doi:10.1038/ngeo1765
- 755 NASA Goddard Space Flight Center, Ocean Ecology Laboratory, Ocean Biology  
756 Processing Group (OBPG). 2015a. Moderate-resolution Imaging  
757 Spectroradiometer (MODIS) Aqua Chlorophyll Data; 2013.1.1 Reprocessing.  
758 NASA OB.DAAC, Greenbelt, MD, USA.  
759 doi:10.5067/AQUA/MODIS/L3M/CHL/2014. Accessed on 2015/01/09.

This is the accepted version of the following article: González-Gil, R., González Taboada, F., Cáceres, C., Largier, J. L. and Anadón, R. (2017), Winter-mixing preconditioning of the spring phytoplankton bloom in the Bay of Biscay. *Limnol. Oceanogr.* doi:10.1002/lno.10769, which has been published in final form at [Limnology & Oceanography](https://doi.org/10.1002/lno.10769). This article may be used for non-commercial purposes in accordance with the [Wiley Self-Archiving Policy](https://doi.org/10.1002/lno.10769).

- 760 NASA Goddard Space Flight Center, Ocean Ecology Laboratory, Ocean Biology  
761 Processing Group (OBPG). 2015b. Sea-viewing Wide Field-of-view Sensor  
762 (SeaWiFS) Chlorophyll Data; 2010.0 Reprocessing. NASA OB.DAAC,  
763 Greenbelt, MD, USA. doi:10.5067/AQUA/MODIS/L3M/CHL/2014. Accessed  
764 on 2015/01/09.
- 765
- 766 Nychka, D., S. Bandyopadhyay, D. Hammerling, F. Lindgren, and S. Sain. 2015. A  
767 Multiresolution Gaussian Process Model for the Analysis of Large Spatial  
768 Datasets. *J. Comput. Graph. Stat.* **24**: 579-599.  
769 doi:10.1080/10618600.2014.914946
- 770 Nychka, D., D. Hammerling, S. Sain, and N. Lenssen. 2016. LatticeKrig: Multiresolution  
771 Kriging Based on Markov Random Fields. R package version 6.2:  
772 [www.image.ucar.edu/LatticeKrig](http://www.image.ucar.edu/LatticeKrig). doi: 10.5065/D6HD7T1R.
- 773
- 774 O'Reilly, J. E. and others. 2000. Ocean color chlorophyll a algorithms for SeaWiFS, OC2,  
775 and OC4: Version 4, p. 9-23. In S. B. Hooker and E. R. Firestone [eds.], *SeaWiFS*  
776 *Postlaunched Calibration and Validation Analyses, Part 3*. NASA Tech. Memo  
777 2000-206892, Vol. 11. NASA, GoddardSpace Flight Center.
- 778 Parsons, T. R., and C. M. Lalli. 1988. Comparative oceanic ecology of the plankton  
779 communities of the subarctic Atlantic and Pacific oceans. *Oceanogr. Mar. Biol.*  
780 *Annu. Rev.* **26**: 317-359.
- 781 Platt, T., C. Fuentes-Yaco, and K. T. Frank. 2003. Spring algal bloom and larval fish  
782 survival. *Nature* **423**: 398-399. doi:10.1038/423398b
- 783 R Core Team. 2017. R: A language and environment for statistical computing. R  
784 Foundation for Statistical Computing, Vienna, Austria. Available from  
785 <http://www.R-project.org/>.
- 786
- 787 Racault, M.-F., C. Le Quéré, E. Buitenhuis, S. Sathyendranath, and T. Platt. 2012.  
788 Phytoplankton phenology in the global ocean. *Ecol. Indicators* **14**: 152-163.  
789 doi:10.1016/j.ecolind.2011.07.010
- 790 Rantajarvi, E., R. Olsonen, S. Hällfors, J.-M. Leppänen, and M. Raateoja. 1998. Effect of  
791 sampling frequency on detection of natural variability in phytoplankton:  
792 unattended high-frequency measurements on board ferries in the Baltic Sea. *ICES*  
793 *J. Mar. Sci.* **55**: 697-704. doi:10.1006/jmsc.1998.0384
- 794 Redfield, A. C. 1958. The biological control of chemical factors in the environment. *Am.*  
795 *Sci.* **46**: 230A-221.
- 796 Reynolds, C. S. 2006. *The ecology of phytoplankton*. Cambridge University Press.

This is the accepted version of the following article: González-Gil, R., González Taboada, F., Cáceres, C., Largier, J. L. and Anadón, R. (2017), Winter-mixing preconditioning of the spring phytoplankton bloom in the Bay of Biscay. *Limnol. Oceanogr.* doi:10.1002/lno.10769, which has been published in final form at [Limnology & Oceanography](https://doi.org/10.1002/lno.10769). This article may be used for non-commercial purposes in accordance with the [Wiley Self-Archiving Policy](https://doi.org/10.1002/lno.10769).

- 797 Reynolds, R. W., T. M. Smith, C. Liu, D. B. Chelton, K. S. Casey, and M. G. Schlax.  
798 2007. Daily high-resolution-blended analyses for sea surface temperature. *J. Clim.*  
799 **20**: 5473-5496. doi:10.1175/2007JCLI1824.1
- 800 RStudio Team. 2016. RStudio: Integrated Development Environment for R. RStudio,  
801 Inc., Boston, MA. Available from <http://www.rstudio.com>.
- 802
- 803 Rumín-Caparrós, A., A. Sanchez-Vidal, C. González-Pola, G. Lastras, A. Calafat, and M.  
804 Canals. 2016. Particle fluxes and their drivers in the Avilés submarine canyon and  
805 adjacent slope, central Cantabrian margin, Bay of Biscay. *Prog. Oceanogr.* **144**:  
806 39-61. doi:<https://doi.org/10.1016/j.pocean.2016.03.004>
- 807 Sambrotto, R. N., H. J. Niebauer, J. J. Goering, and R. L. Iverson. 1986. Relationships  
808 among vertical mixing, nitrate uptake, and phytoplankton growth during the  
809 spring bloom in the southeast Bering Sea middle shelf. *Cont. Shelf Res.* **5**: 161-  
810 198. doi:10.1016/0278-4343(86)90014-2
- 811 Sanders, R. and others. 2014. The biological carbon pump in the North Atlantic. *Prog.*  
812 *Oceanogr.* **129**: 200-218. doi:10.1016/j.pocean.2014.05.005
- 813 Sarmiento, J. L., and N. Gruber. 2006. Ocean biogeochemical dynamics. Princeton  
814 University Press.
- 815 Siegel, D. A., S. C. Doney, and J. A. Yoder. 2002. The North Atlantic spring  
816 phytoplankton bloom and Sverdrup's critical depth hypothesis. *Science* **296**: 730-  
817 733. doi:10.1126/science.1069174
- 818 Sieracki, M. E., P. G. Verity, and D. K. Stoecker. 1993. Plankton community response to  
819 sequential silicate and nitrate depletion during the 1989 North Atlantic spring  
820 bloom. *Deep Sea Res. Part II* **40**: 213-225. doi:10.1016/0967-0645(93)90014-E
- 821 Smayda, T. J. 1970. The suspension and sinking of phytoplankton in the sea. *Oceanogr.*  
822 *Mar. Biol. Annu. Rev.* **8**: 353-414. doi:10.1002/iroh.19720570110
- 823 Smetacek, V. S. 1985. Role of sinking in diatom life-history cycles: ecological,  
824 evolutionary and geological significance. *Mar. Biol.* **84**: 239-251.  
825 doi:10.1007/BF00392493
- 826 Somavilla Cabrillo, R., C. González-Pola, M. Ruiz-Villarreal, and A. Lavín Montero.  
827 2011. Mixed layer depth (MLD) variability in the southern Bay of Biscay.  
828 Deepening of winter MLDs concurrent with generalized upper water warming  
829 trends? *Ocean. Dynam.* **61**: 1215-1235. doi:10.1007/s10236-011-0407-6
- 830 Somavilla, R., C. González-Pola, C. Rodriguez, S. A. Josey, R. F. Sánchez, and A. Lavín.  
831 2009. Large changes in the hydrographic structure of the Bay of Biscay after the  
832 extreme mixing of winter 2005. *J. Geophys. Res.: Oceans* **114**: C01001.  
833 doi:10.1029/2008JC004974

- 834 Sverdrup, H. U. 1953. On conditions for the Vernal Blooming of Phytoplankton. *J. Cons.*  
835 *Int. Explor. Mer.* **18**: 287-295. doi:10.1093/icesjms/18.3.287
- 836 Taboada, F. G., and R. Anadón. 2012. Patterns of change in sea surface temperature in  
837 the North Atlantic during the last three decades: beyond mean trends. *Clim.*  
838 *Change* **115**: 419-431. doi:10.1007/s10584-012-0485-6
- 839 Taylor, J. R., and R. Ferrari. 2011. Shutdown of turbulent convection as a new criterion  
840 for the onset of spring phytoplankton blooms. *Limnol. Oceanogr.* **56**: 2293-2307.  
841 doi:10.4319/lo.2011.56.6.2293
- 842 Townsend, D. W., L. M. Cammen, P. M. Holligan, D. E. Campbell, and N. R. Pettigrew.  
843 1994. Causes and consequences of variability in the timing of spring  
844 phytoplankton blooms. *Deep Sea Res. Part I* **41**: 747-765. doi:10.1016/0967-  
845 0637(94)90075-2
- 846 Ueyama, R., and B. C. Monger. 2005. Wind-induced modulation of seasonal  
847 phytoplankton blooms in the North Atlantic derived from satellite observations.  
848 *Limnol. Oceanogr.* **50**: 1820-1829. doi:10.4319/lo.2005.50.6.1820
- 849 Valdés, L., A. Lavín, M. L. Fernández de Puelles, M. Varela, R. Anadón, A. Miranda, J.  
850 Camiñas, and J. Mas. 2002. Spanish Ocean Observation System. IEO Core  
851 Project: studies on time series of oceanographic data. *Elsevier Oceanogr. Ser.* **66**:  
852 99-105. doi:10.1016/S0422-9894(02)80014-9
- 853 Valdés, L. and others. 2007. A decade of sampling in the Bay of Biscay: What are the  
854 zooplankton time series telling us? *Prog. Oceanogr.* **74**: 98-114.  
855 doi:10.1016/j.pocean.2007.04.016
- 856 Varela, M. 1996. Phytoplankton ecology in the Bay of Biscay. *Sci. Mar.* **60**: 45-53.
- 857 Wickham, H. 2009. *ggplot2: elegant graphics for data analysis*. Springer.
- 858 Williams, R. G., and M. J. Follows. 2003. Physical transport of nutrients and the  
859 maintenance of biological production, p. 19-51. In M. J. R. Fasham [ed.], *Ocean*  
860 *Biogeochemistry: The Role of the Ocean Carbon Cycle in Global Change*.  
861 Springer.
- 862 Wood, S. N. 2006. *Generalized additive models: an introduction with R*. Chapman and  
863 Hall/CRC.
- 864 Wood, S. N., F. Scheipl, and J. J. Faraway. 2013. Straightforward intermediate rank tensor  
865 product smoothing in mixed models. *Stat. Comput.* **23**: 341-360.  
866 doi:10.1007/s11222-012-9314-z
- 867 Yentsch, C. S., and D. W. Menzel. 1963. A method for the determination of  
868 phytoplankton chlorophyll and phaeophytin by fluorescence. *Deep-Sea Res.*  
869 *Oceanogr. Abstr.* **10**: 221-231. doi:10.1016/0011-7471(63)90358-9

- 870 Yoder, J. A., C. R. McClain, G. C. Feldman, and W. E. Esaias. 1993. Annual cycles of  
871 phytoplankton chlorophyll concentrations in the global ocean: A satellite view.  
872 *Glob. Biogeochem. Cycles* **7**: 181-193. doi:10.1029/93GB02358
- 873 Yoshie, N., Y. Yamanaka, M. J. Kishi, and H. Saito. 2003. One dimensional ecosystem  
874 model simulation of the effects of vertical dilution by the winter mixing on the  
875 spring diatom bloom. *J. Oceanogr.* **59**: 563-571.  
876 doi:10.1023/B:JOCE.0000009586.02554.d3
- 877

878        **Acknowledgments**

879        We thank all the people that helped in the establishment and maintenance of the time  
880 series collected at station E3 (Cudillero Transect), especially those from the Areas of  
881 Ecology and Zoology of the University of Oviedo and the entire crew from the research  
882 vessel José Rioja. We also thank NASA Ocean Biology Processing Group (OBPG) and  
883 NOAA National Climatic Data Center (NCDC) for the production, availability and  
884 maintenance of the remote sensing data analyzed in this work. We are especially grateful  
885 to D. Tommasi, A. Rivera and S. Romero for their useful comments. Cudillero time series  
886 are part of the project RADIALES, Instituto Español de Oceanografía (IEO). This is a  
887 contribution of the Asturias Marine Observatory.

888        This research was co-funded by the agreement “Control a largo plazo de las  
889 condiciones químico-biológicas de la Plataforma Continental de Asturias” [Instituto  
890 Español de Oceanografía (IEO) and University of Oviedo] and by the project DOS  
891 MARES (CTM2010-21810- C03-02, Ministerio de Economía y Competitividad,  
892 Gobierno de España). R.G.-G. was supported by a FPU fellowship from the Ministerio  
893 de Educación, Cultura y Deporte, Gobierno de España.



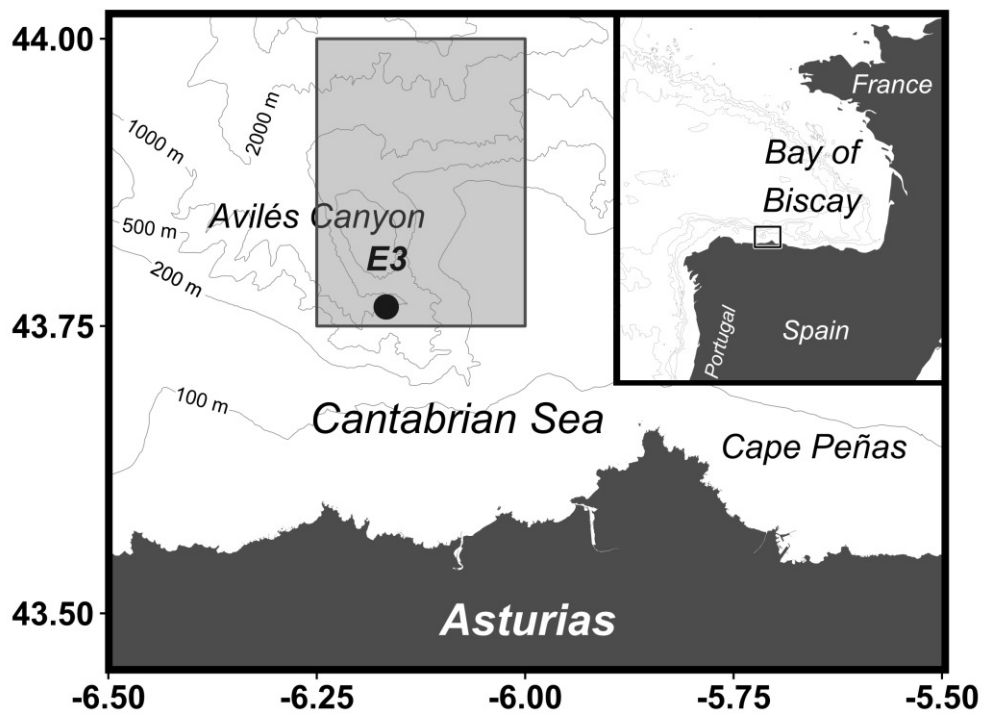


**Fig. 1.** Map of the study area in the central Cantabrian Sea and its position in the Bay of Biscay. The shaded region around station E3 (dot) corresponds to the  $0.25^\circ \times 0.25^\circ$  quadrangle used to average satellite data.

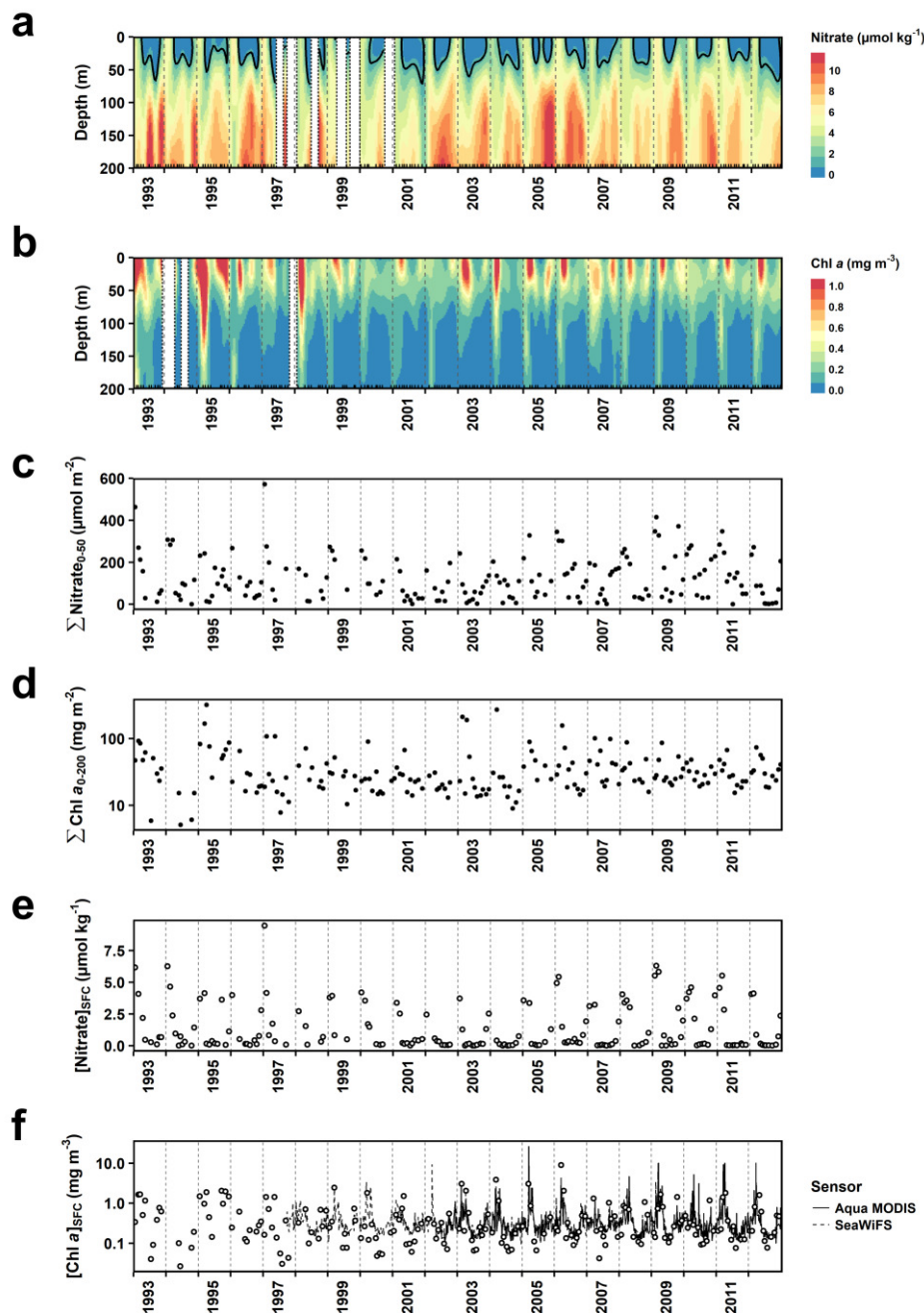


**Fig. 2.** Intra- and interannual variations in: **(a)** nitrate and **(b)** Chl a concentrations over the uppermost 200 m of the water column interpolated using kriging techniques, **(c)** depth-integrated nitrate (0-50 m,  $\Sigma\text{Nitrate}_{0-50}$ ), **(d)** depth-integrated Chl a (0-200 m,  $\Sigma\text{Chl a}_{0-200}$ ), **(e)** surface nitrate concentration ( $[\text{Nitrate}]_{\text{SFC}}$ ) and **(f)** surface Chl a concentration ( $[\text{Chl a}]_{\text{SFC}}$ ) from in situ (dots) and satellite (lines) observations. In all panels, years are separated by gray vertical dashed lines. In **(a)** and **(b)**, inner tick marks on the x-axis indicate those dates when data were collected, and data gaps spanning three or more consecutive months appear as blank stripes delimited by vertical dotted lines. The thick contour line in **(a)** denotes the  $1 \mu\text{mol kg}^{-1}$  nitrate isoline (i.e. the nitracline). Note the use of a  $\log_{10}$  scale for Chl a in panels **(d)** and **(f)**.

895

This is the accepted version of the following article: González-Gil, R., González Taboada, F., Cáceres, C., Largier, J. L. and Anadón, R. (2017), Winter-mixing preconditioning of the spring phytoplankton bloom in the Bay of Biscay. *Limnol. Oceanogr.* doi:10.1002/lno.10769, which has been published in final form at [Limnology & Oceanography](https://doi.org/10.1002/lno.10769). This article may be used for non-commercial purposes in accordance with the [Wiley Self-Archiving Policy](https://doi.org/10.1002/lno.10769).

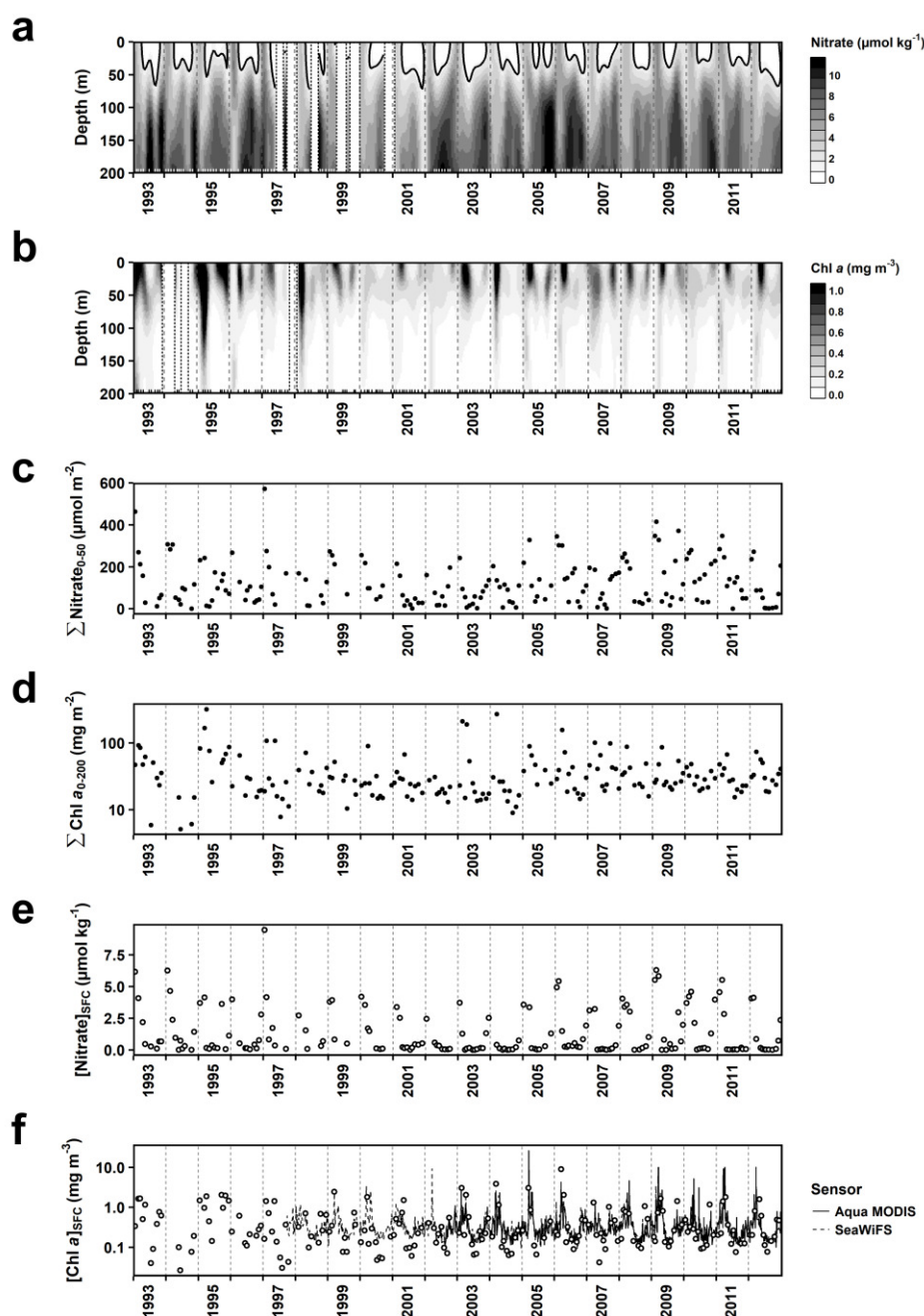


**Fig. 2 (b/w).** Intra- and interannual variations in: **(a)** nitrate and **(b)** Chl a concentrations over the uppermost 200 m of the water column interpolated using kriging techniques, **(c)** depth-integrated nitrate (0-50 m,  $\Sigma$ Nitrate<sub>0-50</sub>), **(d)** depth-integrated Chl a (0-200 m,  $\Sigma$ Chl a<sub>0-200</sub>), **(e)** surface nitrate concentration ( $[\text{Nitrate}]_{\text{SFC}}$ ) and **(f)** surface Chl a concentration ( $[\text{Chl a}]_{\text{SFC}}$ ) from in situ (dots) and satellite (lines) observations. In all panels, years are separated by gray vertical dashed lines. In **(a)** and **(b)**, inner tick marks on the x-axis indicate those dates when data were collected, and data gaps spanning three or more consecutive months appear as blank stripes delimited by vertical dotted lines. The thick contour line in **(a)** denotes the  $1 \mu\text{mol kg}^{-1}$  nitrate isoline (i.e. the nitracline). Note the use of a  $\log_{10}$  scale for Chl a in panels **(d)** and **(f)**.

896

This is the accepted version of the following article: González-Gil, R., González Taboada, F., Cáceres, C., Largier, J. L. and Anadón, R. (2017), Winter-mixing preconditioning of the spring phytoplankton bloom in the Bay of Biscay. *Limnol. Oceanogr.* doi:10.1002/lno.10769, which has been published in final form at [Limnology & Oceanography](https://doi.org/10.1002/lno.10769). This article may be used for non-commercial purposes in accordance with the [Wiley Self-Archiving Policy](https://www.wiley.com/doi/10.1002/lno.10769).

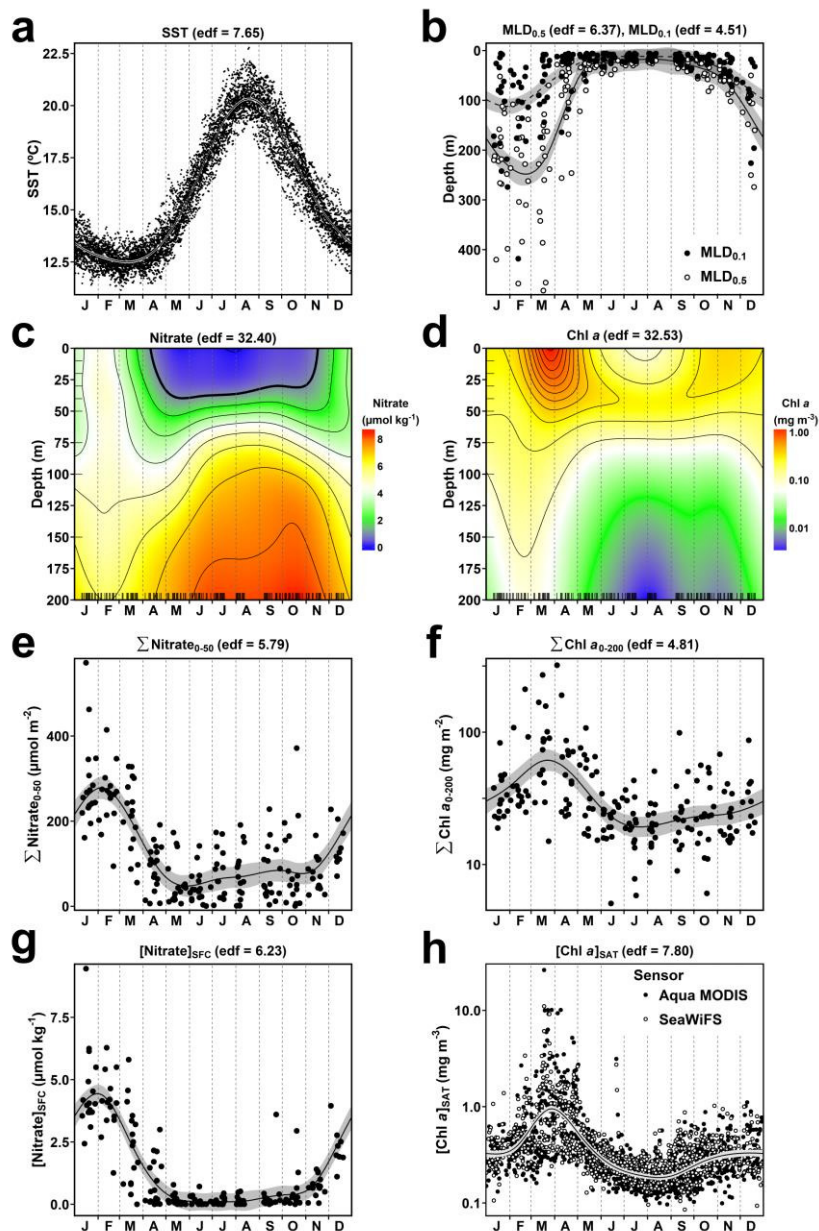


**Fig. 3.** Seasonality of: **(a)** sea surface temperature (SST) based on satellite retrievals, **(b)** mixed layer depth (MLD) calculated using two different criteria (see Material and methods), **(c)** nitrate and **(d)** Chl a concentration over the first 200 m of the water column, **(e)** depth-integrated nitrate (0-50 m,  $\Sigma$ Nitrate<sub>0-50</sub>), **(f)** depth-integrated Chl a (0-200 m,  $\Sigma$ Chl a<sub>0-200</sub>), **(g)** surface nitrate concentration ( $[\text{Nitrate}]_{\text{SFC}}$ ) and **(h)** surface satellite Chl a concentration ( $[\text{Chl a}]_{\text{SAT}}$ ). Observed concentrations or integrated values (dots) and estimated seasonal cycles (solid lines in **a-b** and **e-h** or contour plots in **c-d**) are shown. In **(a-b)** and **(e-h)**, the 95% confidence intervals (shaded areas) associated with the estimated seasonal cycles are shown. Predicted values for each variable are based on the output of the generalized additive models (GAMs). The estimated degrees of freedom (edf) for each model are indicated. The inner tick marks on each axis in **(c)** and **(d)** indicate where data were available. The thick contour line in **(c)** denotes the  $1 \mu\text{mol kg}^{-1}$  nitrate isoline (i.e. the nitracline). Note the use of a  $\log_{10}$  scale for Chl a.

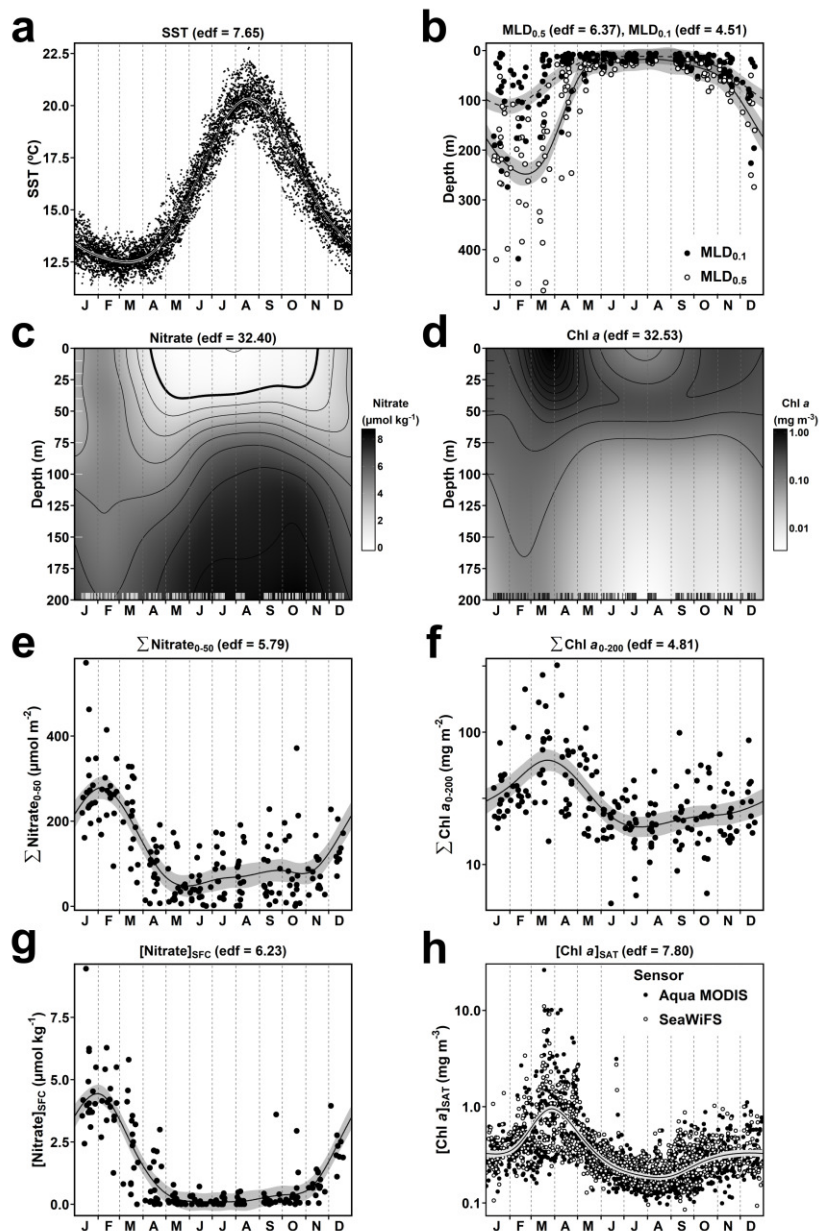


**Fig. 3 (b/w).** Seasonality of: (a) sea surface temperature (SST) based on satellite retrievals, (b) mixed layer depth (MLD) calculated using two different criteria (see Material and methods), (c) nitrate and (d) Chl a concentration over the first 200 m of the water column, (e) depth-integrated nitrate (0-50 m,  $\Sigma$ Nitrate<sub>0-50</sub>), (f) depth-integrated Chl a (0-200 m,  $\Sigma$ Chl a<sub>0-200</sub>), (g) surface nitrate concentration ( $[\text{Nitrate}]_{\text{SFC}}$ ) and (h) surface satellite Chl a concentration ( $[\text{Chl a}]_{\text{SAT}}$ ). Observed concentrations or integrated values (dots) and estimated seasonal cycles (solid lines in a-b and e-h or contour plots in c-d) are shown. In (a-b) and (e-h), the 95% confidence intervals (shaded areas) associated with the estimated seasonal cycles are shown. Predicted values for each variable are based on the output of the generalized additive models (GAMs). The estimated degrees of freedom (edf) for each model are indicated. The inner tick marks on each axis in (c) and (d) indicate where data were available. The thick contour line in (c) denotes the 1  $\mu\text{mol kg}^{-1}$  nitrate isoline (i.e. the nitracline). Note the use of a  $\log_{10}$  scale for Chl a.

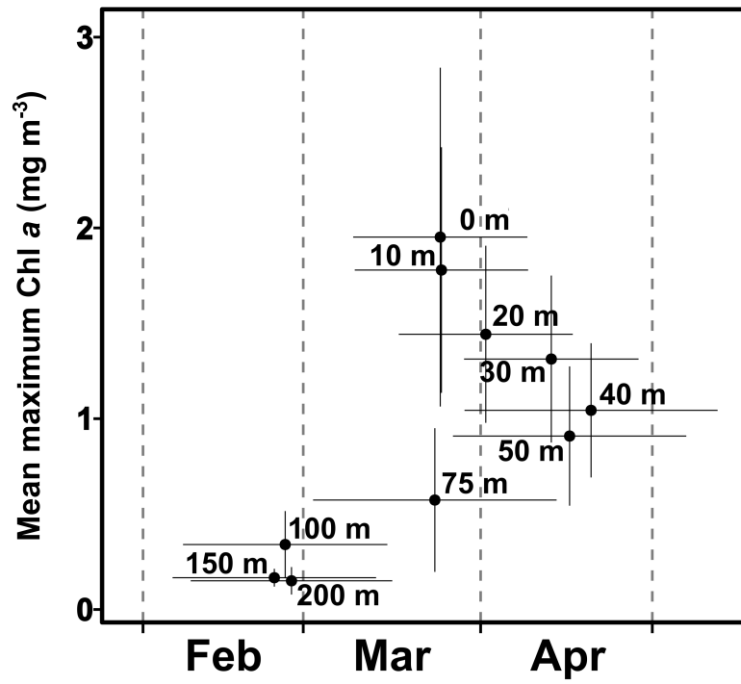


**Fig. 4.** Mean maximum Chl a concentration for each depth during the first half of the year and corresponding mean day of occurrence. Error bars indicate the 95 % confidence interval. Months are delimited by vertical dashed lines.

899

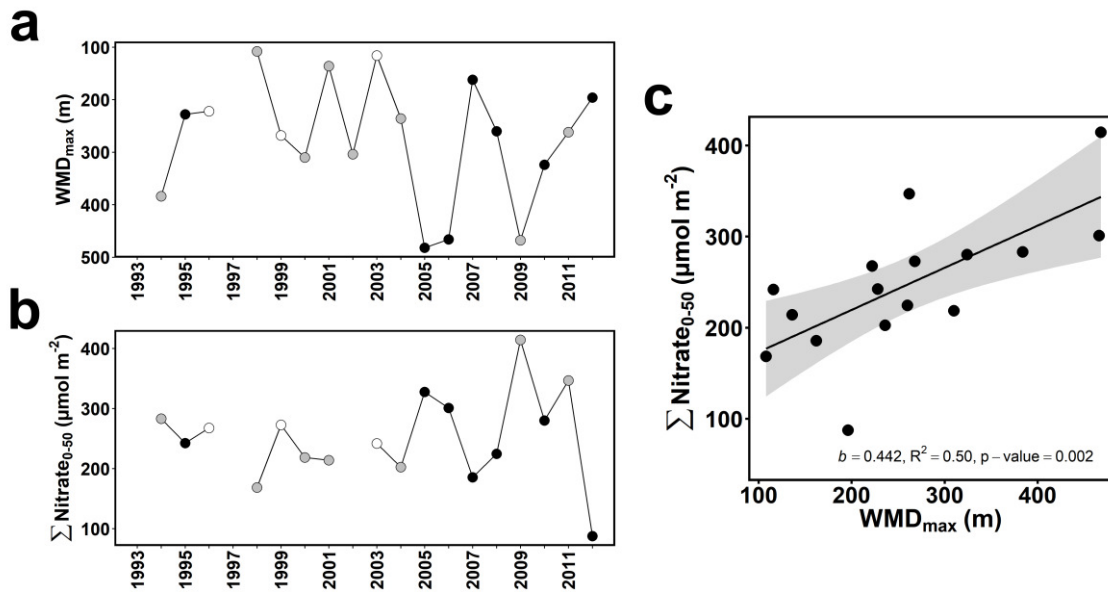


**Fig. 5.** Inter-annual variations of (a) maximum winter mixing depth (WMD<sub>max</sub>) and (b) depth-integrated nitrate (0-50 m, ΣNitrate<sub>0-50</sub>) at the WMD<sub>max</sub> sampling date. Dot color represents the winter month when WMD<sub>max</sub> was measured (white, January; gray, February; black, March). (c) Linear relationship between ΣNitrate<sub>0-50</sub> at the WMD<sub>max</sub> sampling date and WMD<sub>max</sub>. The shaded area represents the 95% confidence interval associated to the linear correlation. The slope (b), proportion of variance explained (R<sup>2</sup>) and p-value of the relationship are shown.

900

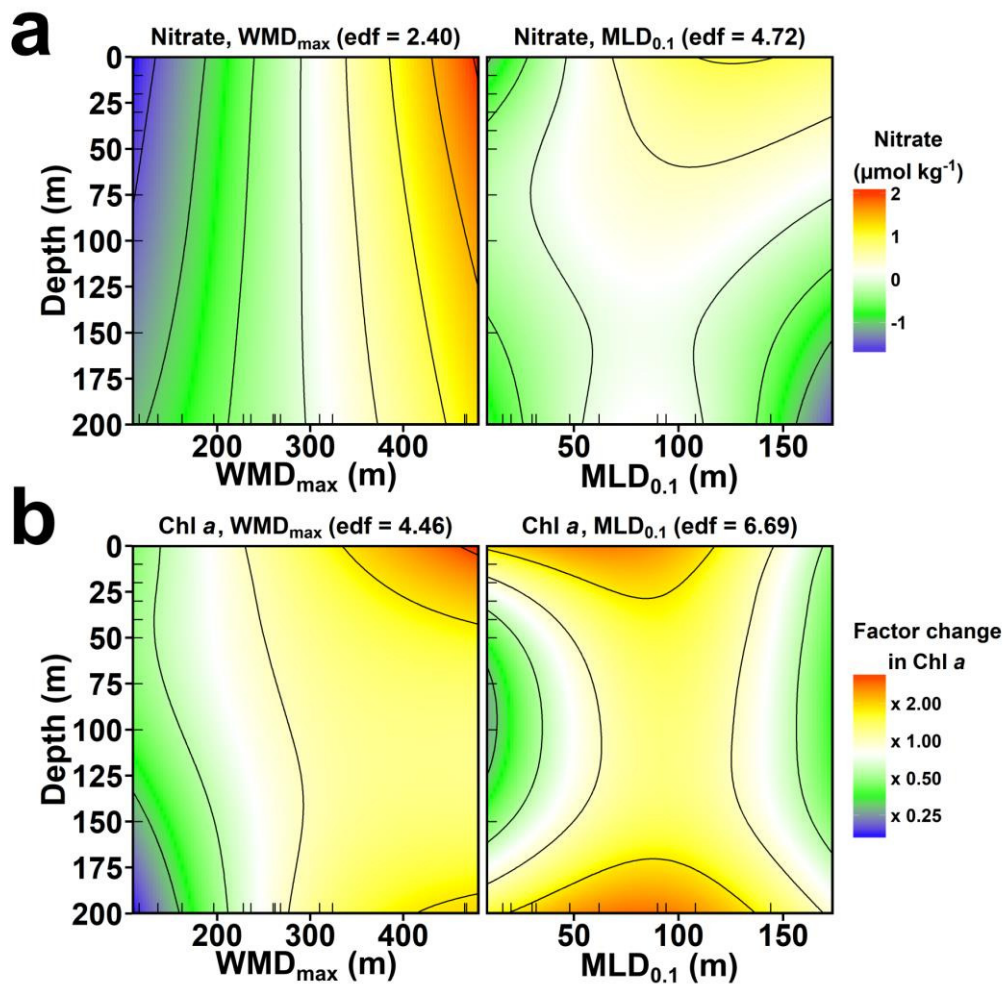


**Fig. 6.** Predicted (a) additive effects on nitrate concentration and (b) multiplicative effects on Chl a concentration of both maximum winter mixing depth (WMD<sub>max</sub>) and near-surface stratification (MLD<sub>0.1</sub>) in March. These values were obtained based on the best generalized additive model (GAM) of a set of proposed models to explore the effect of WMD<sub>max</sub> and MLD<sub>0.1</sub> on nitrate and Chl a concentrations (see Table 1). All terms in the model had a p-value < 0.010 or < 0.050 for nitrate and Chl a concentration, respectively. The estimated degrees of freedom (edf) are also shown. The inner tick marks on each axis indicate where data were available.

901



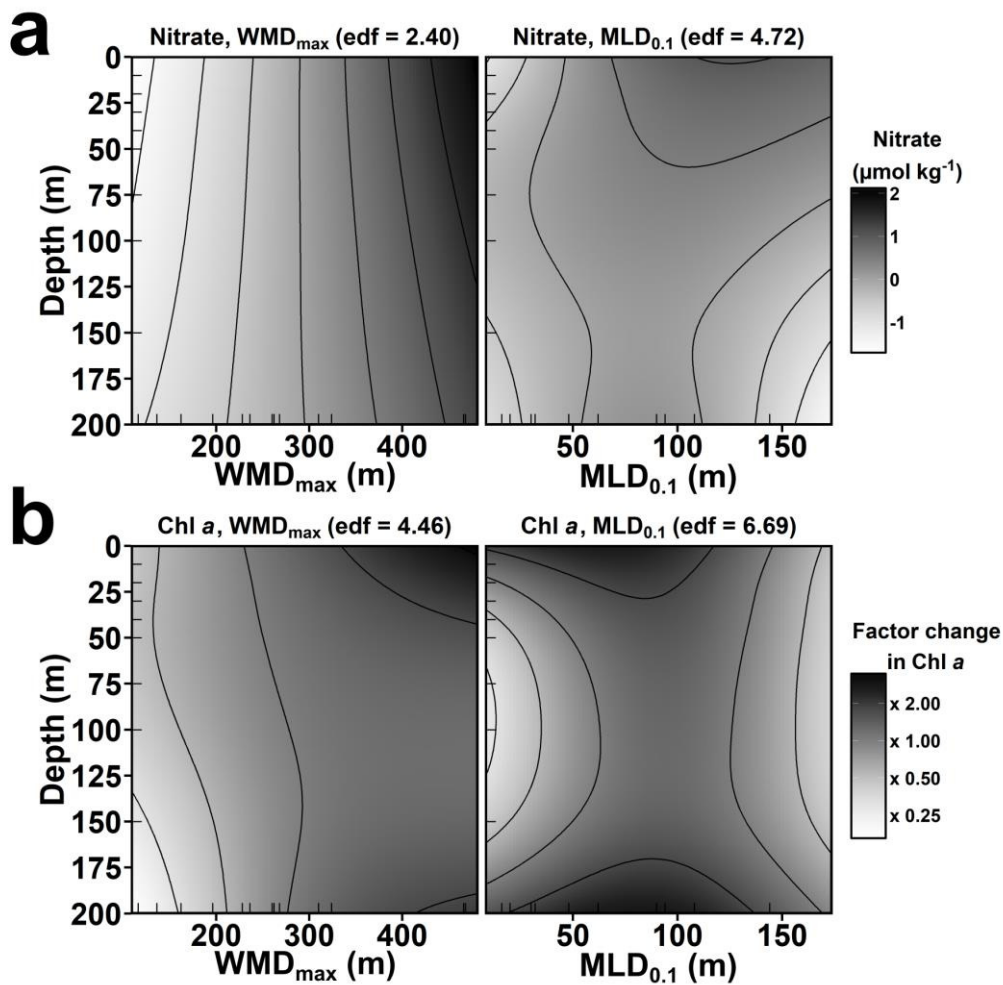


**Fig. 6 (b/w).** Predicted **(a)** additive effects on nitrate concentration and **(b)** multiplicative effects on Chl a concentration of both maximum winter mixing depth ( $WMD_{max}$ ) and near-surface stratification ( $MLD_{0.1}$ ) in March. These values were obtained based on the best generalized additive model (GAM) of a set of proposed models to explore the effect of  $WMD_{max}$  and  $MLD_{0.1}$  on nitrate and Chl a concentrations (see Table 1). All terms in the model had a p-value < 0.010 or < 0.050 for nitrate and Chl a concentration, respectively. The estimated degrees of freedom (edf) are also shown. The inner tick marks on each axis indicate where data were available.

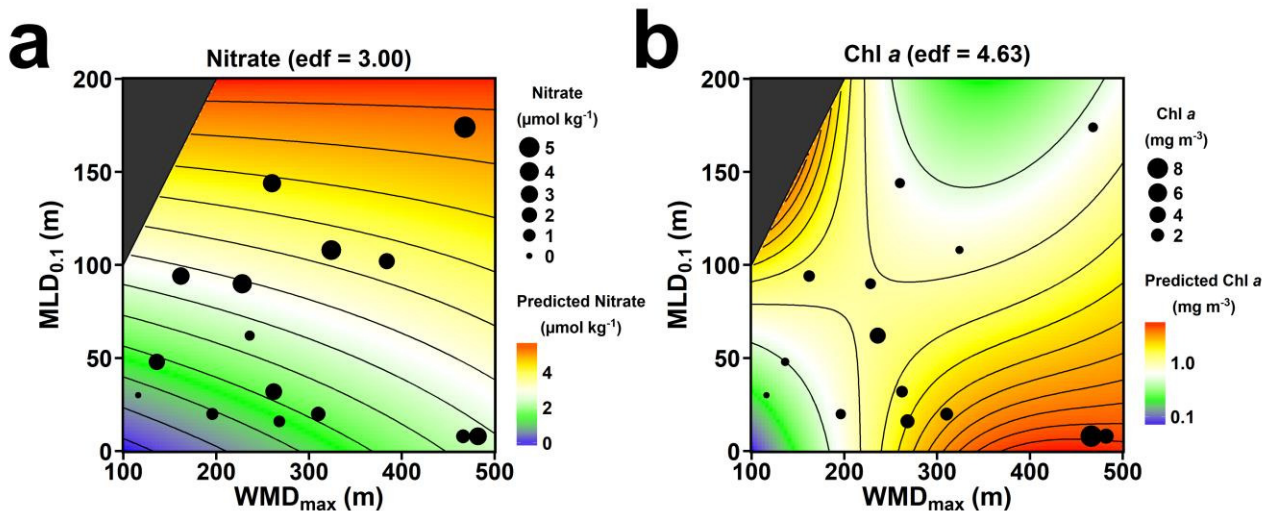


**Fig. 7.** Observed (dot size) and predicted (contour plot) concentrations of (a) nitrate and (b) Chl a at surface (~ 0 m depth) in March. Predicted values were obtained based on the generalized additive model (GAM) in Table 2 that included an interaction term between the maximum winter mixing depth ( $WMD_{max}$ ) and the near-surface stratification depth ( $MLD_{0.1}$ ) in March. This interaction term had a p-value  $< 0.010$  or  $< 0.050$  for nitrate and Chl a concentration, respectively. The estimated degrees of freedom (edf) for each model are indicated. The dark gray triangles on the top left corners delimit those combinations of  $WMD_{max}$  and  $MLD_{0.1}$  that are not possible ( $WMD_{max}$  cannot be shallower than  $MLD_{0.1}$ ). Note that predicted Chl a concentrations are shown in  $\log_{10}$  scale.

903

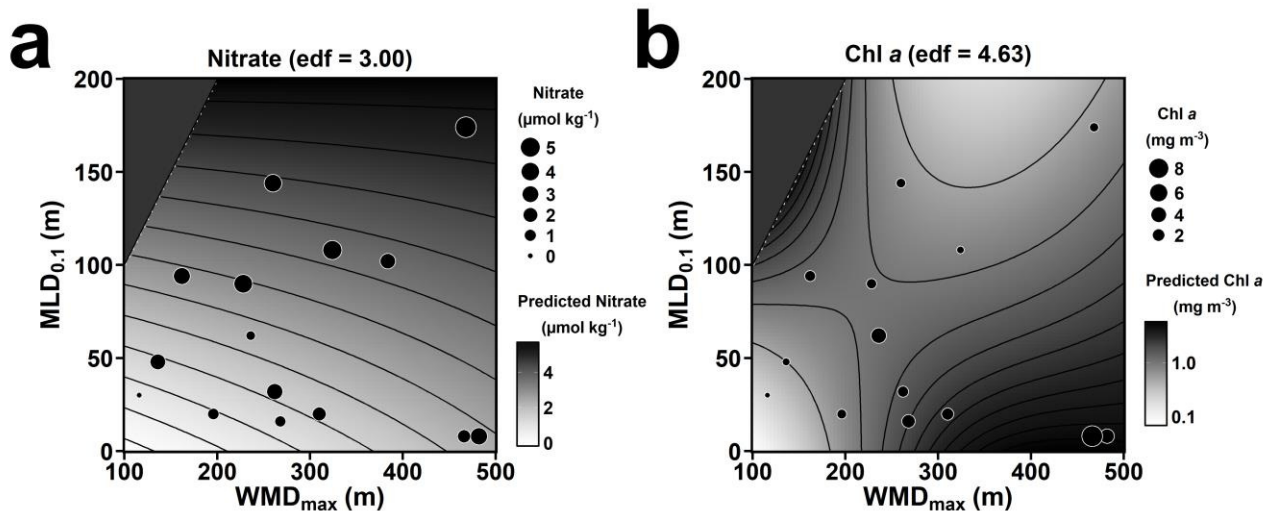


**Fig. 7 (b/w).** Observed (dot size) and predicted (contour plot) concentrations of (a) nitrate and (b) Chl a at surface (~ 0 m depth) in March. Predicted values were obtained based on the generalized additive model (GAM) in Table 2 that included an interaction term between the maximum winter mixing depth (WMD<sub>max</sub>) and the near-surface stratification depth (MLD<sub>0.1</sub>) in March. This interaction term had a p-value < 0.010 or < 0.050 for nitrate and Chl a concentration, respectively. The estimated degrees of freedom (edf) for each model are indicated. The dark gray triangles on the top left corners delimit those combinations of WMD<sub>max</sub> and MLD<sub>0.1</sub> that are not possible (WMD<sub>max</sub> cannot be shallower than MLD<sub>0.1</sub>). Note that predicted Chl a concentrations are shown in log<sub>10</sub> scale.

904

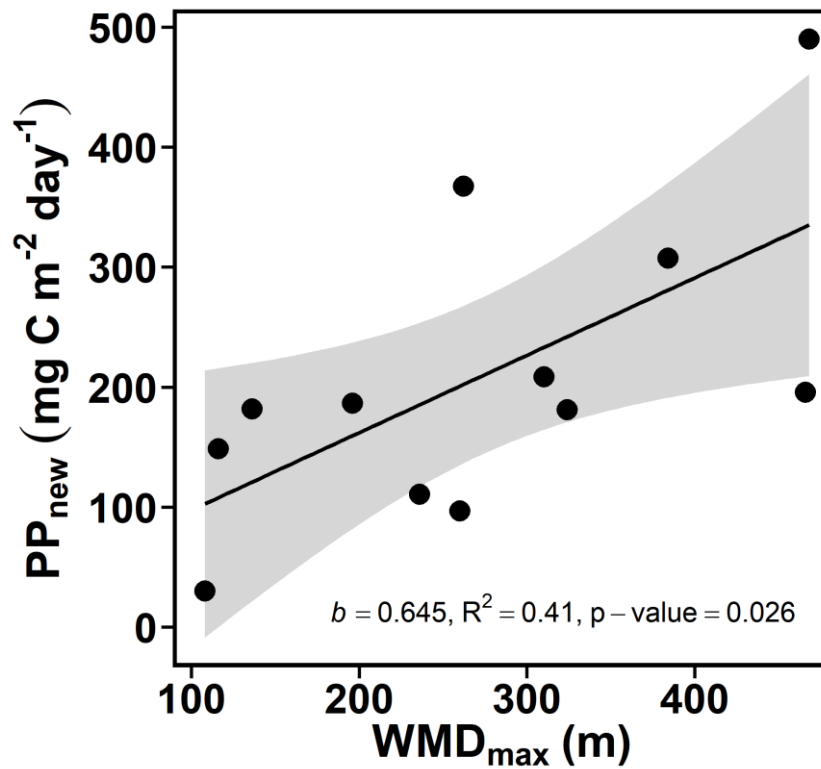


**Fig. 8.** Linear relationship between the new primary production ( $PP_{\text{new}}$ ) in the upper 50 m of the water column between February and April and the maximum winter mixing depth ( $WMD_{\text{max}}$ ). The shaded area represents the 95% confidence interval associated with the linear correlation. The slope ( $b$ ), proportion of variance explained ( $R^2$ ) and p-value of the relationship are shown.

905

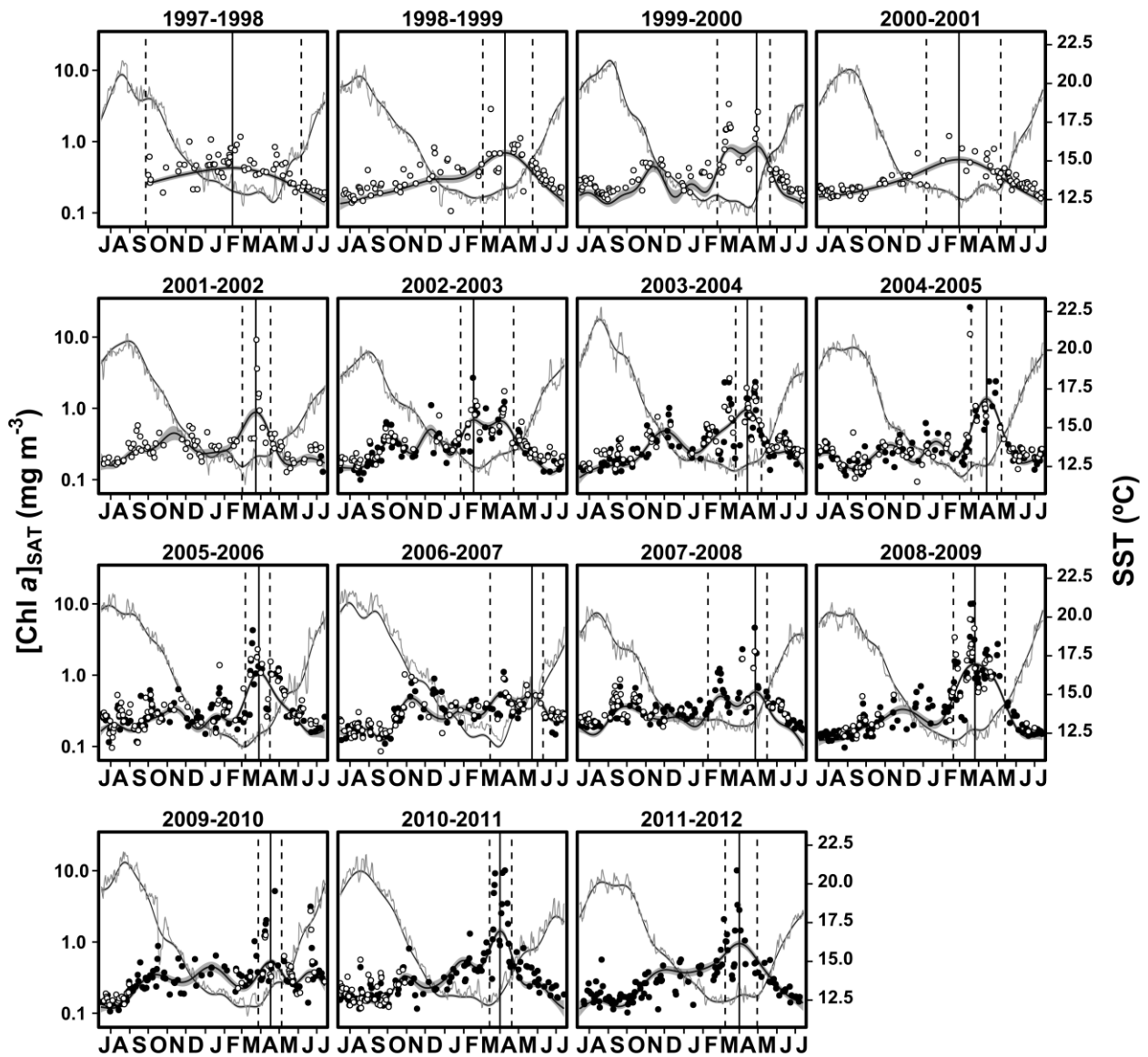


**Fig. 9** Sea surface temperatures (SST, light gray line) and Chl a concentrations ( $[\text{Chl } a]_{\text{SAT}}$ , dots) from 1997 to 2012 based on satellite retrievals. Dot color indicates the sensor used to get the  $[\text{Chl } a]_{\text{SAT}}$  measurements (white for SeaWiFS and black for Aqua MODIS). Estimated seasonal cycles for SST (dark gray line) and  $[\text{Chl } a]_{\text{SAT}}$  (black line) and their associated 95% confidence intervals (shaded areas) are based on the generalized additive model (GAM) predictions. The estimated degrees of freedom (edf) of the model varied between 16.19 and 18.53 for SST or between 3.19 and 13.42 for  $[\text{Chl } a]_{\text{SAT}}$ . Vertical solid lines indicate the maximum estimated  $[\text{Chl } a]_{\text{SAT}}$  during the spring bloom. The initiation and termination day of the spring bloom are marked with vertical dashed lines. Note that  $[\text{Chl } a]_{\text{SAT}}$  is shown in  $\log_{10}$  scale and that the beginning of the seasonal cycle is set to July 15<sup>th</sup> (or 14<sup>th</sup> in a leap year).

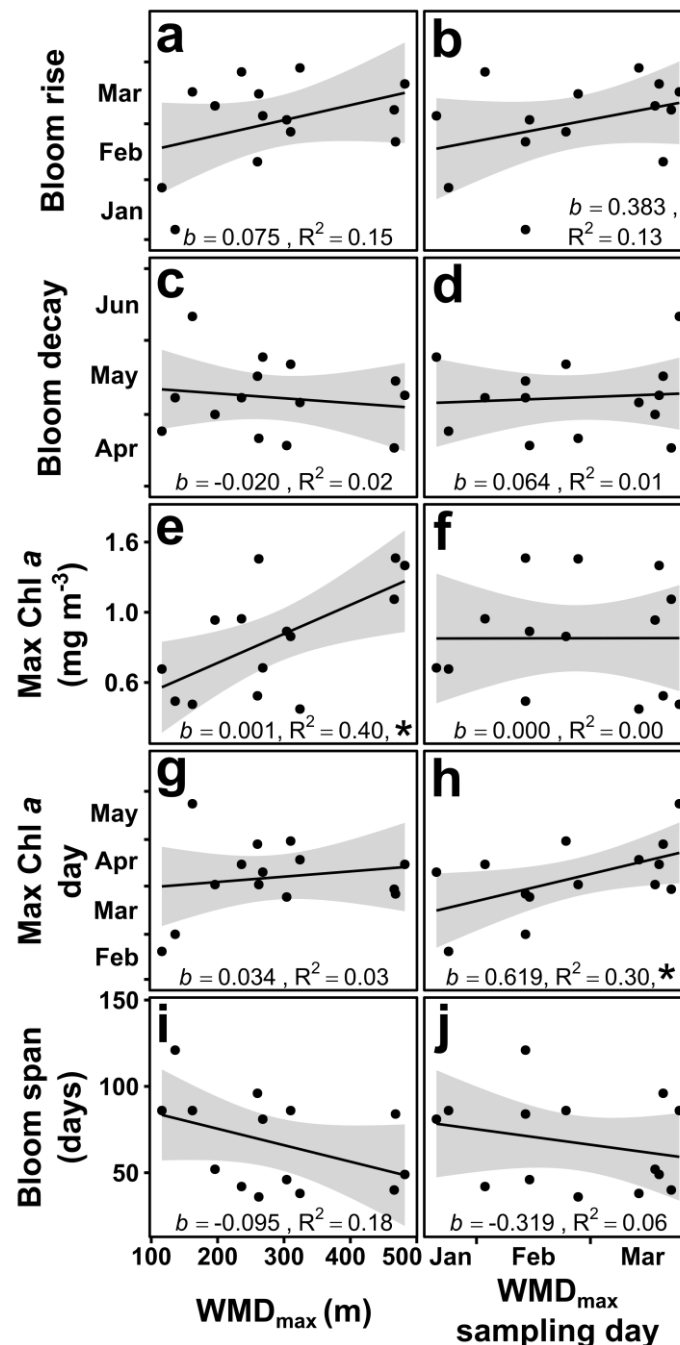


**Fig. 10.** Impact of the intensity and timing of the maximum winter mixing depth ( $WMD_{max}$  and  $WMD_{max}$  sampling date, respectively) on spring bloom metrics: (a-b) bloom rise, (c-d) bloom decay, (e-f) max Chl a, (g-h) max Chl a timing and (i-j) bloom span. The spring bloom metrics were derived from a generalized additive model (GAM) based on satellite data. The shaded areas associated with each linear relationship depict the 95% confidence intervals. The slope (b) and proportion of variance explained ( $R^2$ ) of each relationship are shown. Those linear regressions with a p-value  $< 0.050$  are indicated with a \*. Note that max Chl a is shown in  $\log_{10}$  scale.

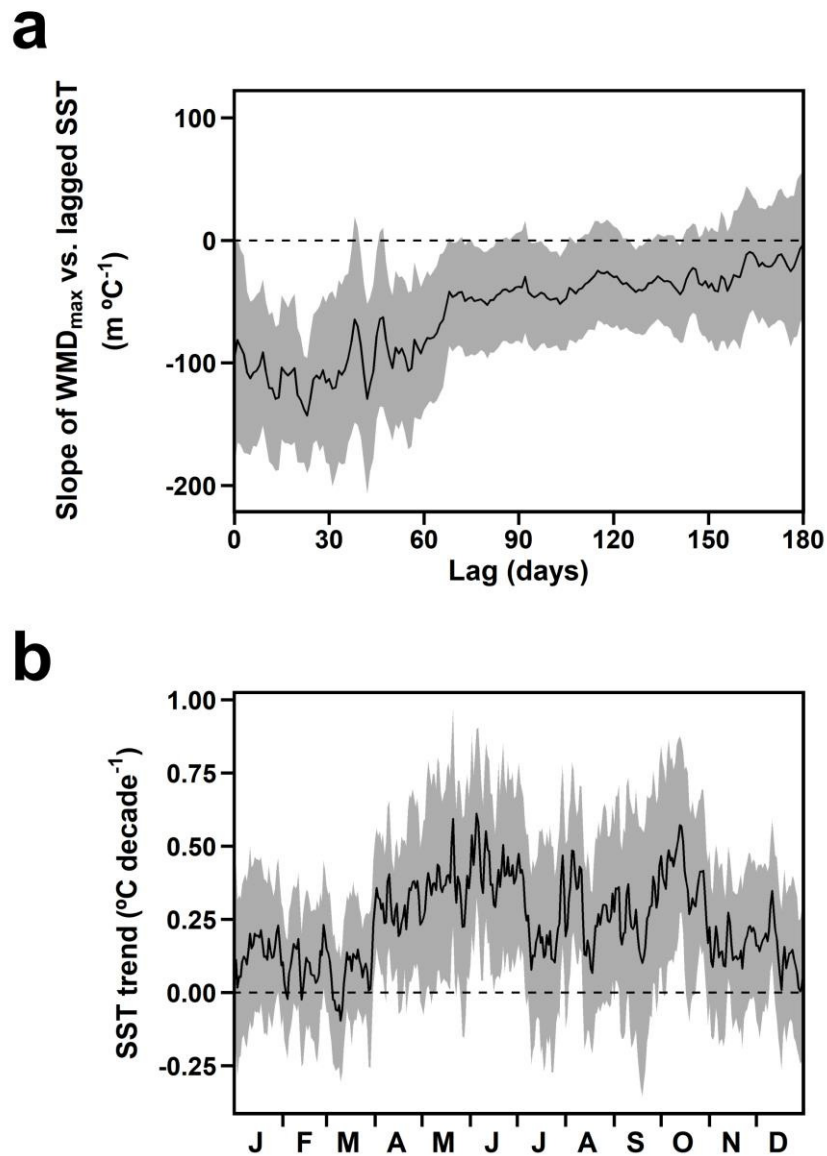


**Fig. 11.** (a) Variations in the slope of the linear relationships between maximum winter mixing depth (WMD<sub>max</sub>) and the Sea Surface Temperature (SST) based on satellite retrievals at different day lags (1993-2012). (b) Long-term linear trends in SST (1981-2012) for each day of the year. Dashed horizontal lines indicate zero values. Shaded areas depict the 95% confidence intervals associated with the regression slopes.

909 **Tables**

910 **Table 1.** Results from the model selection for the assessment of the effect of winter mixing depth ( $WMD_{max}$ ) and our proxy for the thickness of  
 911 the surface stratified layer ( $MLD_{0.1}$ ) on nitrate and Chl a concentration at all depths (both represented as  $y$  in the formulas) in March. All models  
 912 included an intercept ( $a$ ) and an error term ( $\varepsilon$ ). In addition, the generalized additive models (GAMs) incorporated through a smooth function ( $f$ ,  
 913 see Supporting information for further details) the influence of depth ( $z$ ), or also the effect of the interaction ( $te$ ) between  $MLD_{0.1}$  or  $WMD_{max}$  and  
 914 depth. We report for each model the Akaike Information Criterion (AIC) and its associated weight (Burnham and Anderson 2002), and the  
 915 proportion of variance explained ( $R^2$ ). In all cases, the overall model had a p-value  $< 0.001$ .

Model	What does the model estimate?	Nitrate			Chl a		
		AIC	AIC weight	R <sup>2</sup>	AIC	AIC weight	R <sup>2</sup>
$y = a + \varepsilon$	Null model (includes only an intercept).	598.80	0.00	0.00	222.61	0.00	0.00
$y = a + f(z) + \varepsilon$	Effect of depth.	534.20	0.00	0.36	139.50	0.00	0.47
$y = a + f(z) + te(WMD_{max}, z) + \varepsilon$	Effect of winter mixing through the water column while accounting for the influence of depth.	452.09	0.00	0.64	122.99	0.00	0.56
$y = a + f(z) + te(MLD_{0.1}, z) + \varepsilon$	Effect of stratification through the water column while accounting for the influence of depth.	513.04	0.00	0.48	131.77	0.00	0.54
$y = a + f(z) + te(MLD_{0.1}, z) + te(WMD_{max}, z) + \varepsilon$	Combined effect of stratification and winter mixing through the water column while accounting for the influence of depth.	419.50	1.00	0.73	101.29	1.00	0.65

This is the accepted version of the following article: González-Gil, R., González Taboada, F., Cáceres, C., Largier, J. L. and Anadón, R. (2017), Winter-mixing preconditioning of the spring phytoplankton bloom in the Bay of Biscay. *Limnol. Oceanogr.* doi:10.1002/lno.10769, which has been published in final form at [Limnology & Oceanography](#). This article may be used for non-commercial purposes in accordance with the [Wiley Self-Archiving Policy](#).



916 **Table 2.** Results from the model selection for the assessment of the effect of winter mixing depth ( $WMD_{max}$ ) and our proxy for the thickness of  
 917 the surface stratified layer ( $MLD_{0.1}$ ) on nitrate and Chl a concentration (both represented as  $y$  in the formulas) at the surface ( $\sim 0$  m depth) in March.  
 918 All models included an intercept ( $a$ ) and an error term ( $\varepsilon$ ). In addition, the generalized additive models (GAMs) incorporated a smooth function ( $f$   
 919 see Supporting information for further details) to estimate the effect of  $WMD_{max}$ ,  $MLD_{0.1}$  or their interaction ( $te$ , last model). We report for each  
 920 model the Akaike Information Criterion (AIC) and its associated weight (Burnham and Anderson 2002), and the proportion of variance explained  
 921 ( $R^2$ ). The p-values for the overall model are also shown.

Model	What does the model estimate?	Nitrate				Chl a			
		AIC	AIC weight	$R^2$	p-value	AIC	AIC weight	$R^2$	p-value
$y = a + \varepsilon$	Null model (includes only an intercept).	60.63	0.00	0.00	0.000	20.12	0.00	0.00	0.572
$y = a + f(WMD_{max}) + \varepsilon$	Effect of winter mixing.	59.92	0.00	0.17	0.132	17.42	0.02	0.29	0.049
$y = a + (MLD_{0.1}) + \varepsilon$	Effect of stratification.	51.51	0.21	0.52	0.002	19.78	0.01	0.15	0.165
$y = a + f(MLD_{0.1}) + f(WMD_{max}) + \varepsilon$	Independent combined effect of stratification and winter mixing.	49.70	0.53	0.63	0.003	15.14	0.06	0.48	0.030
$y = a + te(WMD_{max}, MLD_{0.1}) + \varepsilon$	Interactive combined effect of winter mixing and stratification.	51.16	0.26	0.64	0.008	9.72	0.91	0.75	0.016

922

This is the accepted version of the following article: González-Gil, R., González Taboada, F., Cáceres, C., Largier, J. L. and Anadón, R. (2017), Winter-mixing preconditioning of the spring phytoplankton bloom in the Bay of Biscay. *Limnol. Oceanogr.* doi:10.1002/lno.10769, which has been published in final form at [Limnology & Oceanography](#). This article may be used for non-commercial purposes in accordance with the [Wiley Self-Archiving Policy](#).